Acta Pharmaceutica Sinica B 2025;15(8):4078−4095

Chinese Pharmaceutical Association
Institute of Materia Medica, Chinese Academy of Medical Sciences

Acta Pharmaceutica Sinica B

www.elsevier.com/locate/apsb
www.sciencedirect.com

ORIGINAL ARTICLE

Macrophage DGKζ-mediated phosphatidic acid remodeling aggravates acute liver failure

Yumeng Miao[a,b,†], Tzuchun Lin[a,†], Bianlin Wang[c,†], Junyu Xu[b,†], Chongxian Li[d], Zuopeng Li[c], Xinwen Zhang[b], Chendong Zhou[b], Tuerganaili Aji[e], Minjia Tan[b,*], Haji Akber Aisa[c,e,*], Jingya Li[b,d,*]

[a]*Department of Cardiology, Shanghai Institute of Cardiovascular Diseases, Zhongshan Hospital, Fudan University, Shanghai 200032, China*
[b]*Shanghai Institute of Materia Medica, Chinese Academy of Sciences, Shanghai 201203, China*
[c]*Xinjiang Technical Institute of Physics and Chemistry, Chinese Academy of Sciences, Urumqi 830011, China*
[d]*School of Chinese Materia Medica, Nanjing University of Chinese Medicine, Nanjing 210023, China*
[e]*The First Affiliated Hospital of Xinjiang Medical University, Urumqi 830054, China*

Received 8 November 2024; received in revised form 10 February 2025; accepted 11 April 2025

KEY WORDS

Xanthohumol derivative;
Macrophages;
Acute liver failure;
Diacylglycerol kinase ζ;
Phosphatidic acid;
Signal transducer and activator of transcription 3;
Interleukin-1β;
Inflammation

Abstract Acute liver failure (ALF) is a life-threatening condition associated with macrophage-mediated inflammatory responses. Effective therapies and drugs are still lacking to date. Here, we reveal that a derivative of xanthohumol, CAM12203, alleviates lipopolysaccharide (LPS) + D-galactosamine (D-GalN)-induced ALF through limiting macrophage-mediated inflammation, with the most significant impact on interleukin-1β (IL-1β) transcription. Through biotin labeling-mediated pull-down and LC−MS/MS analysis, diacylglycerol kinase ζ (DGKζ), a lipid-metabolizing kinase, is identified as the direct target of CAM12203. Mechanistically, DGKζ is induced in macrophages upon inflammatory stimuli and is upregulated observed on clinical liver failure samples. Its product phosphatidic acid (PA) boosts phospholipase C (PLC)−inositol 1,4,5-trisphosphate (IP_3)−Ca^{2+} signaling and subsequent janus kinase 2 (JAK2)−signal transducer and activator of transcription 3 (STAT3) cascade, ultimately promoting IL-1β production and liver failure. DGKζ knockdown/ablation or inhibition significantly impairs the DGKζ−STAT3−IL-1β pathway along with ALF progression. Finally, CAM12203 is confirmed to be a new DGKζ inhibitor and acts against inflammation in a DGKζ-reliant manner. Taken together, CAM12203 inhibits IL-1β transcription in macrophages by binding to DGKζ and blocking the DGKζ

*Corresponding authors.
E-mail addresses: mjtan@simm.ac.cn (Minjia Tan), haji@ms.xjb.ac.cn (Haji Akber Aisa), jyli@simm.ac.cn (Jingya Li).
†These authors made equal contributions to this work.

Peer review under the responsibility of Chinese Pharmaceutical Association and Institute of Materia Medica, Chinese Academy of Medical Sciences.

https://doi.org/10.1016/j.apsb.2025.06.019

−STAT3 axis, thereby exerting an ameliorative effect on ALF. These results not only highlight CAM12203 as a promising lead compound for ALF treatment, but also define DGKζ as a novel therapeutic target.

1. Introduction

Acute liver failure (ALF), a serious liver damage and sudden deterioration of liver function caused by viruses, drugs, alcohol, chemicals, toxins, hepatic ischemia−reperfusion injury, autoimmune hepatitis, etc., is a life-threatening condition with a tremendous morbidity rate as high as 30%[1,2]. Symptomatic and supportive managements are applied for ALF currently. In a considerable proportion of cases, however, targeted therapies and disease-specific drugs are not available to prevent death, where liver transplantation constitutes the sole medical mean. Despite the effectiveness, the performance is limited by a shortage of donors, a burden of expensive costs, surgical challenges, and a requirement for life-long immune suppression[3,4]. Therefore, it is of utmost need to apply the knowledge generated from the pathogenesis of ALF towards the exploration of directed therapies and novel therapeutic drugs.

It has been recognized that local and circulatory components of the immune system make the responses to acute hepatic insults. When activated by pathogen- and damage-associated molecular patterns from injured hepatocytes, liver-resident macrophages (Kupffer cells, KCs) produce substantial quantities of proinflammatory cytokines and chemokines, leading to the recruitment of peripheral monocytes, which differentiate into monocyte-derived macrophages (MoMFs) within the liver microenvironment. The secreted factors from these macrophages act through an autocrine/paracrine fashion not only to amplify the inflammatory cascade, but also activate the apoptotic signals in hepatocytes[5−8]. Interleukin-1β (IL-1β), one of the proinflammatory cytokines released during the early stage of an inflammatory response, leads to the infiltration of neutrophils along with other macrophages, triggering and exacerbating liver damage[9]. The complex interplay among kinases, signal transducers, and transcriptional factors shapes the uncontrolled transcriptional network of proinflammatory effectors, including IL-1β, with nuclear factor-κB (NF-κB) and signal transducer and activator of transcription 3 (STAT3) being the principal pathways involved[10,11]. Macrophages depletion, NF-κB/STAT3 inhibition, IL-1β knockdown/knockout significantly cause disease remission in a lipopolysaccharide (LPS) + D-galactosamine (D-GalN)-induced ALF model[12−16], indicating that macrophage-mediated inflammatory responses lie at the nexus of ALF development, and intervention in macrophage−IL-1β axis is an effective approach for ALF treatment.

Over the past decades, the immunometabolism field, which reveals the enticing link between energetic metabolism and immune cells, has flourished with a fast-growing number of papers. The connection between cellular metabolism and macrophage responses is not limited to solving the energy demands of the cells. In particular, metabolic intermediates and associated enzymes of lipid metabolism interact with and regulate the transcriptional network of macrophage effectors, thereby ensuring the acquisition of context-dependent functional outcomes[17,18]. This concept applies to saturated very long chain ceramides as well as ceramide synthase 2 which enforce NF-κB family-dependent IL-1β gene expression[19] and desmosterol-mediated transrepression of such proinflammatory factors[20], etc., providing a fresh perspective focusing on lipid metabolism for the studies of macrophage-directed intervention in ALF.

Xanthohumol (XN), a prenylated chalcone isolated from *Humulus lupulus* L. (hops), exhibits multiple biological activities[21]. A large body of evidence has also confirmed its effect against inflammation: it decreases the levels of IL-1β, tumor necrosis factor-α (TNF-α), and monocyte chemoattractant protein-1 (MCP-1) in LPS-stimulated U937 and RAW264.7 cells, and exerts ameliorative effects on experimental colitis and lung injury[22−25]. Our previous work has illustrated that a derivative of XN, named CAM12203, exerts a greater anti-inflammatory efficacy than its precursor[26], suggesting a considerable potential for future development. In this study, we determined that CAM12203 alleviates ALF through limiting macrophage-mediated inflammation. Diacylglycerol kinase ζ (DGKζ), a lipid-metabolizing enzyme that generates phosphatidic acid (PA) from diacylglycerol (DAG), is demonstrated to drive IL-1β production in macrophages and subsequent ALF *via* STAT3 activation, and is identified as the target protein of CAM12203. Overall, our results dissect the action mode of this XN derivative against inflammation, and provide macrophage DGKζ as a novel target for ALF therapy.

2. Materials and methods

2.1. Reagents

CAM12203 and its biotinylated probe were synthesized and provided by Xinjiang Technical Institute of Physics and Chemistry (See the Supporting Information for details). BAY 2965501 (HY-153343), Stattic (HY-13818), BAPTA-AM (HY-100545), 2-APB (HY−W009724), and U73122 (HY-13419) were purchased from MedChemExpress (Monmouth Junction, USA). Control Liposomes (phosphate-buffered saline (PBS)) (40338ES08) and Clodronate Liposomes (40337ES08) were purchased from Yeasen (Shanghai, China). Fluo-4 AM (S1060) was purchased from Beyotime (Shanghai, China). Alanine transaminase (ALT) (290703), aspartate transferase (AST) (290705), and lactate dehydrogenase (LDH) (290717) assay kits were purchased from Sysmex (Kobe, Japan). Mouse IL-1β ELISA kit (VAL601) and HTRF kit (62MIL1BPEG) were purchased from Novus Biologicals (Littleton, USA) and PerkinElmer (Waltham, USA), respectively.

2.2. Animals

C57BL/6J mice (male, 7−8-week-old) were purchased from Beijing HFK Bio-Technology Co., Ltd. (Beijing, China). DGKζ KO (*Dgkz*$^{-/-}$) mice (Strain No. T028497) were purchased from

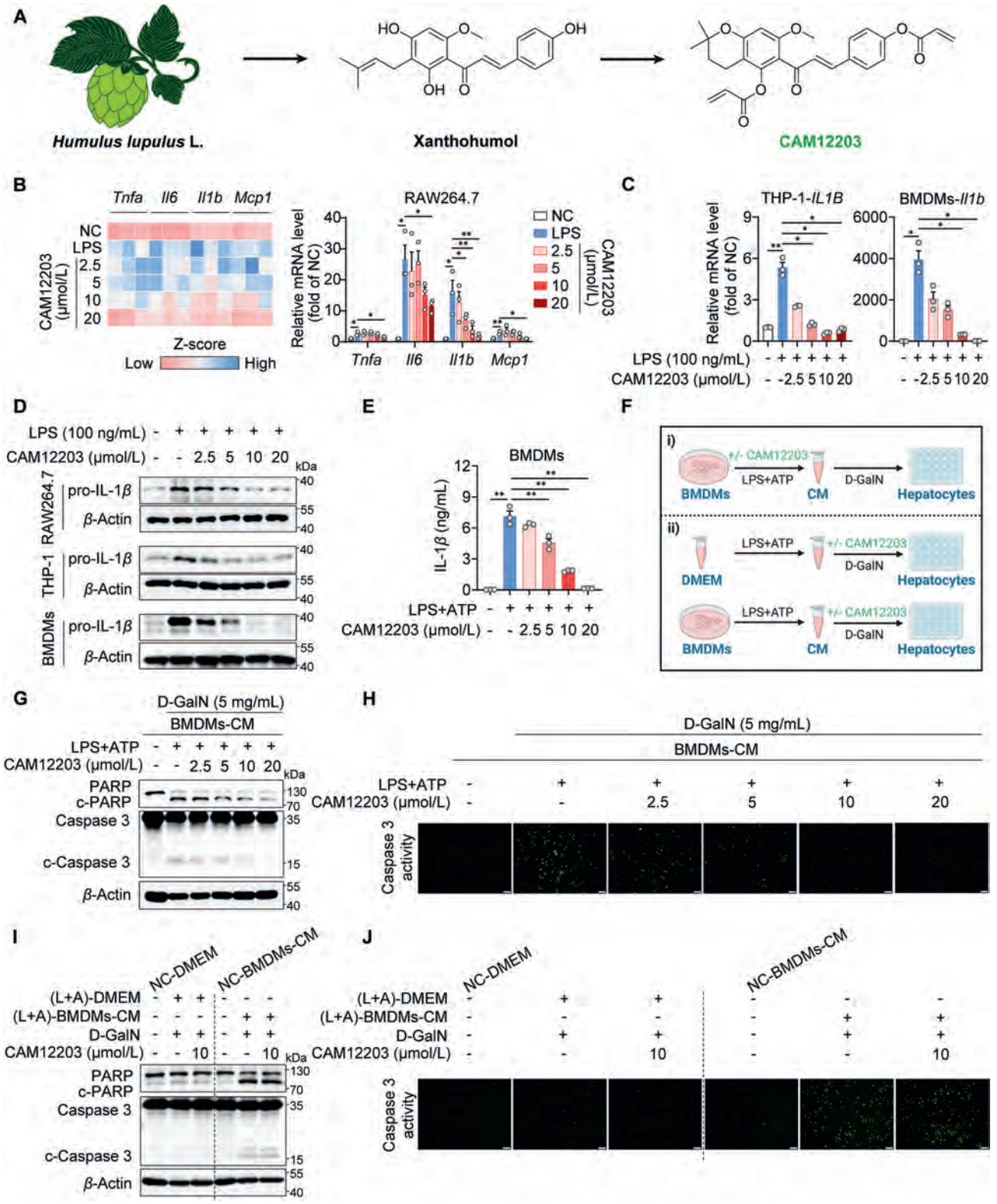

Figure 1 CAM12203 inhibits macrophage-mediated inflammation and liver cell apoptosis. (A) Structure of xanthohumol and CAM12203 (created with Biorender.com). (B) RAW264.7 cells (with or without CAM12203 pretreatment for 2 h) were stimulated with LPS for 4 h. The mRNA levels of proinflammatory factors were detected by Q-PCR. (C) PMA-differentiated THP-1 cells and BMDMs (with or without CAM12203 pretreatment for 2 h) were stimulated with LPS for 4 h. The mRNA level of *IL1B*/*Il1b* was detected by Q-PCR. (D) RAW264.7, PMA-differentiated THP-1 cells, and BMDMs (with or without CAM12203 pretreatment for 2 h) were stimulated with LPS for 4 h. The protein level of pro-IL-1β was determined by Western blotting. (E) BMDMs (with or without CAM12203 pretreatment for 2 h) were stimulated with LPS (4 h) + ATP (another 45 min). The IL-1β concentration in culture medium (CM) was examined by HTRF. (F) Flow chart of the induction of

GemPharmatech (Nanjing, China). All animals were allowed access to a standard laboratory diet under an environment of 12 h light/dark (22 ± 2 °C). The animal treatments were following the instructions of Guide for Care and Use of Laboratory Animals from NIH, and were approved by the Animal Ethics Committee of the Shanghai Institute of Materia Medica (approval number: 2022-04-LJY-91; 2023-05-LJY-122; 2024-04-LJY-147).

2.3. Human liver tissue collection

Paraffin-embedded human liver sections from acute-on-chronic liver failure (ACLF) patients and Healthy Controls were provided by the First Affiliated Hospital of Xinjiang Medical University. The informed consent was obtained from each subject for the experimentation. The collection of human samples during hepatic resection or liver transplantation and the experiments performed adhered strictly to the ethical principles outlined in the Declaration of Helsinki, and were approved by the First Affiliated Hospital ethics committee of Xinjiang Medical University (approval number: 231124-04).

2.4. Cell culture

RAW264.7, THP-1, and HEK293T cells were provided by the Cell Bank of Shanghai. Among them, RAW264.7 and HEK293T cells were maintained in DMEM (10% fetal bovine serum (FBS)), while THP-1 cells were maintained in RPMI 1640 (10% FBS) and induced into macrophages with phorbol 12-myristate 13-acetate (PMA) (100 ng/mL; HY-18739, MedChemExpress) for 24 h. Bone marrow cells were isolated[27] and generated into bone marrow-derived macrophages (BMDMs) by incubation with DMEM containing 10% FBS as well as macrophage colony-stimulating factor (M-CSF) (20 ng/mL; RP01216, ABclonal) for 7 days.

2.5. Cell viability

Cell viability was examined following the manufacturer's instructions for CCK-8. In detail, the cells were cultured for 24 h with CAM12203. CCK-8 (10 μL per well; MA0225, Meilun Biotechnology, Dalian, China) was added during the last hour, and the optical absorbance value at 450 nm was measured.

2.6. Q-PCR

Total RNAs were extracted by RNAiso Plus (9109, Takara, Shiga, Japan) and were reversely transcribed to cDNAs by using RT SuperMix (R323, Vazyme, Nanjing, China). Then, the cDNAs were evaluated with Q-PCR Master Mix (RK21205, ABclonal, Wuhan, China) and primers (Supporting Information Table S1) for Q-PCR assay.

2.7. Western blotting

The samples underwent SDS-PAGE were transferred, blocked, and incubated with primary antibodies overnight (4 °C) and secondary antibodies for 1.5 h (room temperature) sequentially, followed by visualization with enhanced chemiluminescent reagent. Primary antibodies applied included DGKζ (1:1000; ab239080) which was obtained from Abcam (Cambridge, UK), proline rich tyrosine kinase 2 (Pyk2) (1:3000; 17592-1-AP), DGKα (1:2000; 11547-1-AP), DGKε (1:1000; 11900-1-AP), DGKθ (1:500; 17885-1-AP) and β-Actin (1:8000; 66009-1-Ig) which were obtained from Proteintech (Wuhan, China), DGKγ (1:500; DF13919) which was obtained from Affinity (Cincinnati, USA), DGKδ (1:500; A15115) and α-Tubulin (1:1000; A6830) which were obtained from Ablconal, IL-1β (1:1000; 12242), poly-ADP-ribose-polymerase (PARP) (1:1000; 9542), Caspase 3 (1:1000; 9662), p65 (1:1000; 8242), pp65 (1:1000; 3033), STAT3 (1:1000; 9139), $pSTAT3^{Ser727}$ (1:1000; 9134), $pSTAT3^{Tyr705}$ (1:2000; 9145), and pPyk2 (1:1000; 3291) which were obtained from Cell Signaling Technology (Danvers, USA), janus kinase 2 (JAK2) (1:1000; AF1489) and pJAK2 (1:500; AF5854) which were obtained from Beyotime, suppressor of cytokine signaling-1 (SOCS1) (1:500; WL05128) and SOCS3 (1:1000; WL01364) which were obtained from Wanleibio (Shenyang, China).

2.8. Evaluation of hepatocyte damage

Mouse primary hepatocytes were isolated as pervious described[27], and incubated with culture medium (CM) from LPS (100 ng/mL; 4 h; L2630, Sigma−Aldrich, St. Louis, MO, USA) + ATP (2 mmol/L; another 45 min; A2383, Sigma−Aldrich)-stimulated BMDMs plus additional D-GalN (5 mg/mL; G0500, Sigma−Aldrich). After 16 h, Caspase 3 activity in hepatocytes was measured by a commercial GreenNuc™ Caspase 3 assay kit (C1168M, Beyotime) according to the instructions. Moreover, cell lysates were prepared for Western blotting assay of cleaved-PARP and cleaved-Caspase 3 after a 24 h-incubation.

2.9. Immunoprecipitation

RAW264.7 cells were lysed with NP40 (P0013F, Beyotime), supplied with a protease inhibitor cocktail (HY-K0010, MedChemExpress). Protein A/G magnetic beads (20 μL; HY-K0202, MedChemExpress) were added to the protein supernatant for a 30 min-incubation on a rotating wheel to remove the nonspecific binding. Then, the supernatant was collected and rotated with 2 μg Pyk2 antibody overnight (4 °C), followed by another 4 h-rotation (room temperature) with protein A/G magnetic beads (50 μL). The washed immunoprecipitates were measured by Western blotting.

2.10. Pull-down assay

Protein solution from RAW264.7 cells was pretreated with or without CAM12203 (300 μmol/L) for 2 h (4 °C), followed by incubation with the biotin probe (10 μmol/L) derived from CAM12203 for another 2 h (4 °C). Each sample was added with 40 μL streptavidin magnetic beads (HY-K0208,

hepatocyte damage (created with Biorender.com). (G, H) BMDMs were treated with or without CAM12203, followed by LPS + ATP stimulation. The CM was collected and added to the primary hepatocytes along with D-GalN. The levels of cleaved-PARP (c-PARP) and cleaved-Caspase 3 (c-Caspase 3) (G), and the activity of Caspase 3 (scar bar: 100 μm) (H) were determined. (I, J) BMDMs were stimulated by LPS + ATP, and the CM was collected. The primary hepatocytes were incubated with the CM or DMEM along with D-GalN in the presence or absence of CAM12203. The levels of c-PARP and c-Caspase 3 (I), and the activity of Caspase 3 (scar bar: 100 μm) (J) were determined. Data are displayed as mean ± SEM ($n = 3$). *$P < 0.05$, **$P < 0.01$ *vs*. the indicated group.

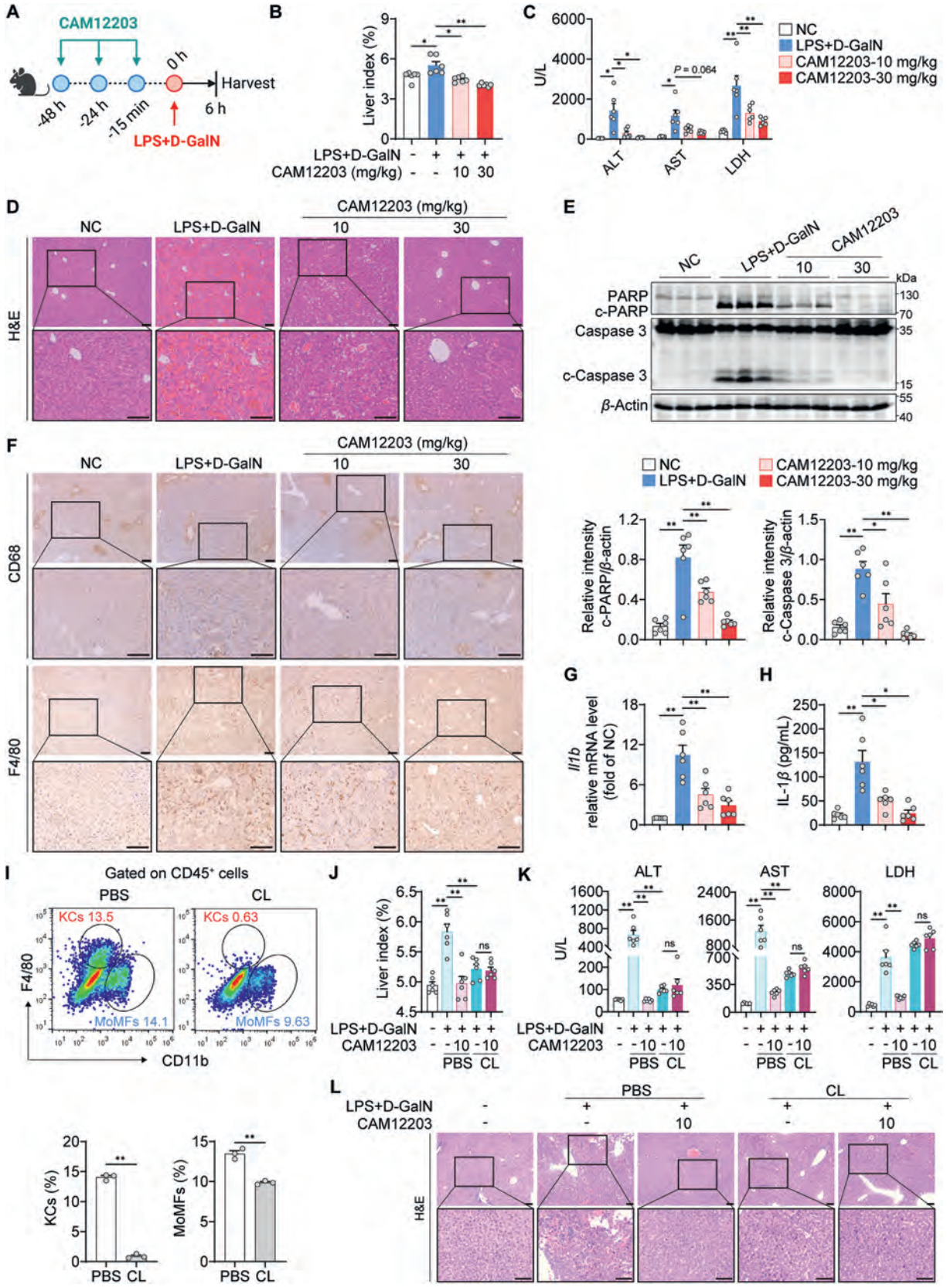

Figure 2 CAM12203 protects against ALF in mice. (A) Overall scheme of the preventive administration study for CAM12203 (created with Biorender.com). (B) The liver index was calculated. (C) The levels of ALT, AST, and LDH in plasma were measured. (D) The histological alterations were evaluated by H&E staining (scar bar: 100 μm). (E) The levels of cleaved-PARP (c-PARP) and cleaved-Caspase 3 (c-Caspase 3) in the liver were determined by Western blotting. (F) Macrophages in the liver were marked by CD68 or F4/80 staining (scar bar: 100 μm). (G) The

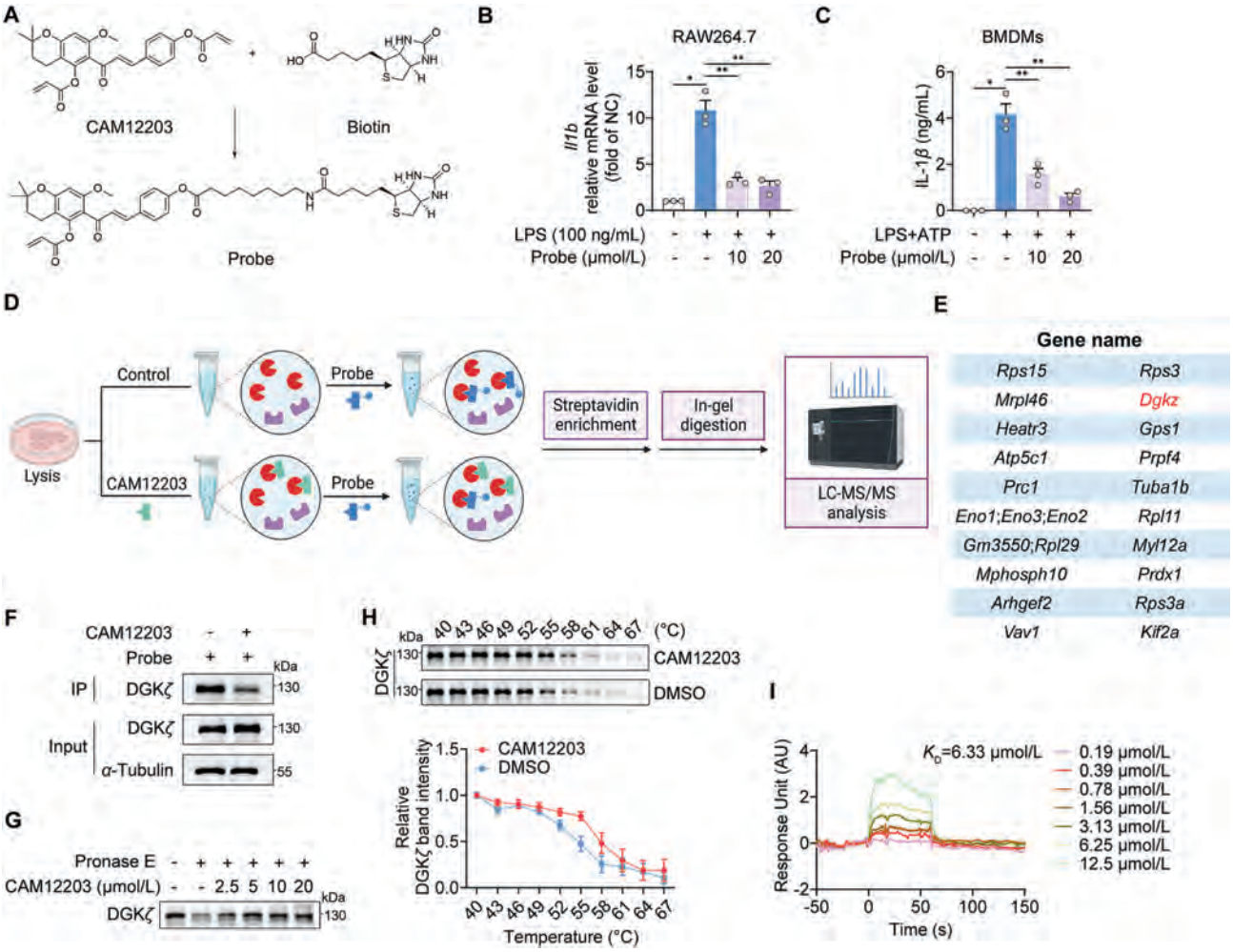

Figure 3 CAM12203 directly binds to DGKζ. (A) Structure of the biotinylated probe. (B) RAW264.7 cells (pretreated with or without the probe for 2 h) were stimulated with LPS for 4 h. The mRNA level of *Il1b* was detected by Q-PCR. (C) BMDMs (pretreated with or without the probe for 2 h) were stimulated with LPS (4 h) + ATP (another 45 min). The IL-1β concentration in culture medium (CM) was examined by HTRF. (D) Overall scheme of the experiments to identify the targets of CAM12203 (created with Biorender.com). (E) The list of gene names of CAM12203-binding proteins. (F) RAW264.7 lysate was pretreated with or without CAM12203 for 2 h (4 °C), followed by incubation with the probe for another 2 h (4 °C). The level of DGKζ pulled down was determined by Western blotting. (G) RAW264.7 lysate was treated with or without CAM12203, and the protein stability of DGKζ resistant to pronase E was determined by DARTS. (H) RAW264.7 lysate was treated with or without CAM12203, and the thermostability of DGKζ was determined by CETSA. (I) DGKζ protein was treated with CAM12203, and the binding affinity was determined by SPR. Data are displayed as mean ± SEM ($n = 3$). $^*P < 0.05$, $^{**}P < 0.01$ *vs*. the indicated group.

MedChemExpress) and rotated for 4 h (4 °C). Then, the pull-down beads were collected and washed with PBST for 4 times. The final samples were separated by SDS-PAGE.

2.11. *In-gel trypsin digestion*

The protein bands from SDS-PAGE were excised. After being destained in 50% ethanol and washed in ddH_2O, the gels containing the protein were cut into fine pieces, and then dehydrated in acetonitrile. Then, the pieces were reduced in dithiothreitol (10 mmol/L) for 40 min (56 °C), and alkylated in iodoacetamide (55 mmol/L) for 40 min (room temperature). After that, the gel samples were washed sequentially in ammonium bicarbonate (100 mmol/L) and 50% acetonitrile/ammonium bicarbonate solution. The dried samples were digested overnight (37 °C) by trypsin and then extracted with 50% acetonitrile/5% trifluoroacetic acid, 75% acetonitrile/0.1% trifluoroacetic acid, and pure acetonitrile, sequentially.

mRNA level of *Il1b* in the liver was detected by Q-PCR. (H) The IL-1β concentration in plasma was measured by ELISA. (I) The efficiency of macrophage elimination in mice intravenously injected with control liposomes (PBS) or clodronate liposomes (CL) was analyzed by the flow cytometric method after 24 h. (J−L) Mice were preventively administered with CAM12203, and PBS or CL was intravenously injected 24 h before the LPS + D-GalN induction. After induction for 6 h, the mice were harvested. The liver index (J), the levels of ALT, AST, and LDH in plasma (K), and the histological alterations of the liver (scar bar: 100 μm) (L) were evaluated. Data are displayed as mean ± SEM ($n = 6$). $^*P < 0.05$, $^{**}P < 0.01$ *vs*. the indicated group; ns, not significant.

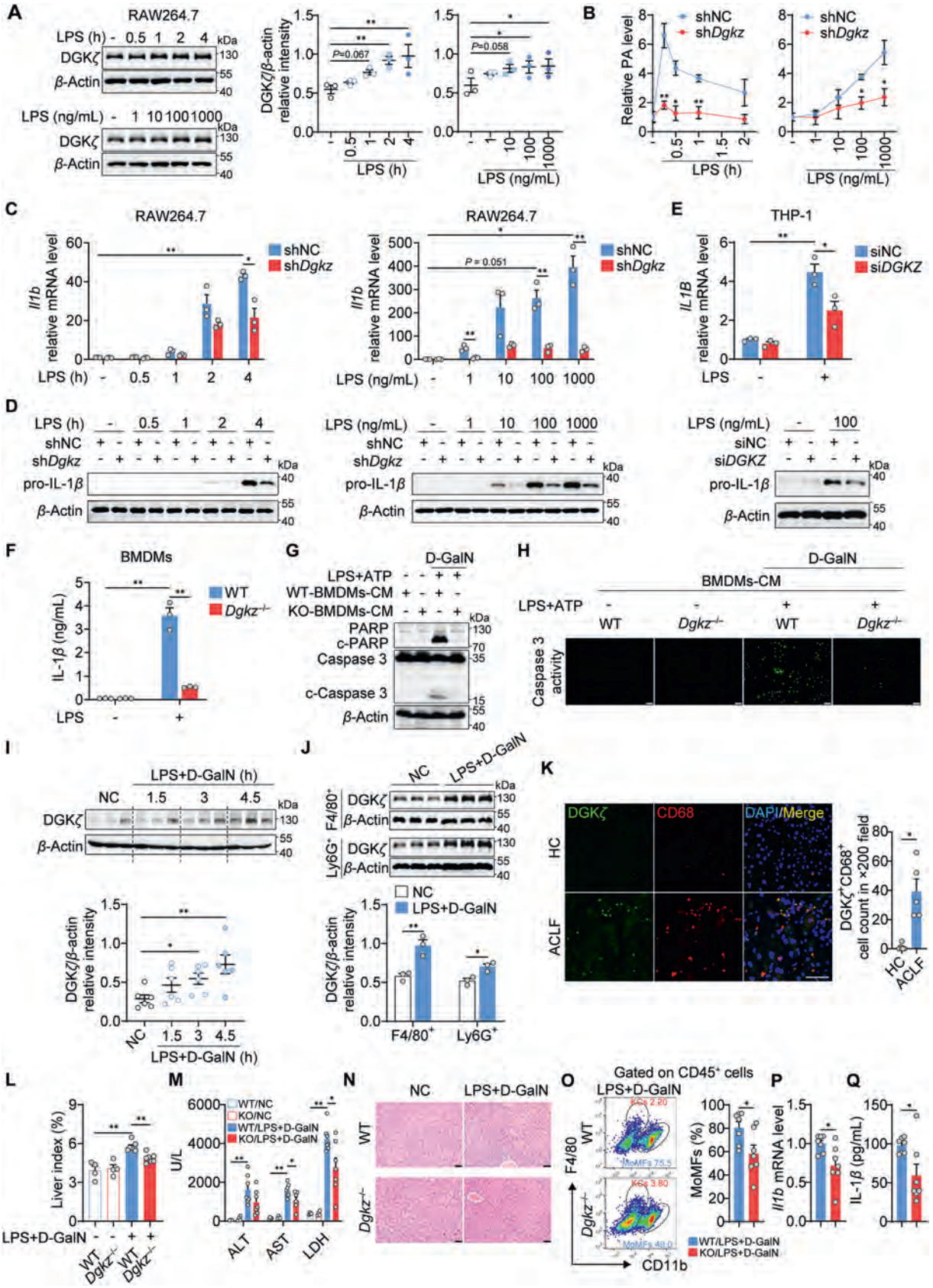

Figure 4 DGKζ plays a critical role in macrophage-mediated inflammation and liver failure. (A) The protein level of DGKζ in LPS-stimulated RAW264.7 cells was determined by Western blotting. (B—D) Stable shNC- and sh*Dgkz*-RAW264.7 cells were stimulated with LPS. The level of PA (B) and IL-1β expression (C, D) were measured by a commercial kit, Q-PCR, and Western blotting, respectively. (E) PMA-differentiated THP-

2.12. LC−MS/MS

The tryptic peptide samples were solved in buffer A (0.1% formic acid, 2% acetonitrile), and were analyzed in a Q Exactive HF-X-Easy-nLC 1200 system at 300 nL/min through a 65 min linear gradient from 5% to 80% buffer B (0.1% formic acid, 90% acetonitrile). A mass resolution of 60,000 at 350−1400 *m*/*z* was set. The automatic gain control (AGC) was set at 5.0×10^6 for Orbitrap. Ions were isolated and fragmented in the HCD model with an NCE of 28% for MS2 scans. The dynamic exclusion duration was set to 30 s.

2.13. Quantitative proteomic analysis

The raw data from Q Exactive HF-X were searched against the UniProt Mus musculus database in MaxQuant (version 1.5.3.8). The trypsin/P was set as the protease, and up to 2 missed cleavages were allowed. Carbamidomethyl (C) was set as the fixed modification, and oxidation (M) along with acetylation (Protein N-term) were added as variable modifications. The iBAQ values were used for protein quantitation[28]. Proteins identified in 2 of 3 biological replicates (iBAQ values with fold-change >1.5 in the "probe" group compared to "CAM12203+probe" group, or proteins only identified in the "probe" group) were considered as potential targets of CAM12203.

2.14. Cellular thermal shift assay (CETSA)

Cells were lysed by liquid nitrogen snap freeze, and the lysates were centrifuged for 20 min (4 °C, 14,000×*g*). The soluble fraction was divided equally into two tubes, followed by treatment with CAM12203 (10 μmol/L) or DMSO for 1 h (room temperature). Afterwards, the mixture was further divided into 50 μL aliquots and heated for 3 min at the indicated temperature. The samples cooled to room temperature were spun down for 20 min (4 °C, 14,000×*g*). The supernatant was collected and measured by Western blotting.

2.15. Drug affinity responsive target stability (DARTS)

Lysates were divided into six 50 μL-aliquots, including one control (PBS) aliquot. The remaining aliquots were incubated with CAM12203 for 2 h (room temperature). Pronase E (1 μg/mL; 1074330001, Sigma−Aldrich) was added to each aliquot except the control group for another 10 min-reaction (room temperature), which was ceased by loading buffer. The final samples were measured by Western blotting.

2.16. Surface plasmon resonance (SPR)

For the SPR experiment, 6 × His-tagged, recombinant full-length human DGKζ (expressed in HEK293T cells, purified by Ni-NTA His-Tag purification agarose (HY−K0210, MedChemExpress)) was prepared. The S-series sensor chip CM5 (29149603, Cytiva) was employed to achieve a response of 20−30 response units by optimizing the protein concentration and contact time. The measurements were carried out on a Biacore T200 instrument in running buffer (10 mmol/L HEPES pH 7.4, 150 mmol/L NaCl) at 30 μL/min, 25 °C. Increasing concentrations of CAM12203 (0.19, 0.39, 0.78, 1.56, 3.13, 6.25, 12.5 μmol/L) were injected into the same surface for 60 s. After the dissociation of the compound from the protein, the surface was washed with running buffer for 180 s. The SPR sensorgrams equilibrium dissociation constant (K_D) was analyzed in Biacore T200 evaluation software (surface-bound analysis settings) or fitted by GraphPad Prism (one site-specific binding). SPR sensorgrams and saturation curves were prepared in GraphPad Prism.

2.17. Lentivirus production and knockdown

Endogenous DGKζ in RAW264.7 cells was depleted using shRNA *via* a lentiviral system. Primers' sequences are: sh*Dgkz*-F (CACC GCTTCACCATGACATCCTTGGTTCAAGAGACCAAGGATG TCATGGTGAAGC) and sh*Dgkz*-R (AAAAGCTTCACCATGA ATCCTTGGTCTCTTGAACCAAGGATGTCATGGTGAAGC). To obtain stable cell lines, RAW264.7 cells were infected for 24 h with the lentiviral supernatants from HEK293T cells co-transfected with lentiviral transfer vector (pCDH), psPAX2, and pMD2.G. The cells were selected with Blasticidin S hydrochloride (5 μg/mL; HY-103401, MedChemExpress), and the knockdown efficiency was measured by Western blotting.

2.18. Transient transfection

Small interfering RNA of human DGKζ (si*DGKZ*) (sense: CGACAAGUCUUCGACCUGA(dT) (dT); anti-sense: UCAG-GUCGAAGACUUGUCG(dT) (dT)) and Lipofectamine 3000 (L3000015, Invitrogen, Carlsbad, CA, USA) were added respectively to equal amounts of Opti-MEM. Then, the mixed complex was added to the cells for a 24 h-incubation (37 °C). In some cases, the DGKζ overexpression plasmid was transfected into cells with Lipofectamine 3000 and P3000. The transfection efficiency was measured by Western blotting.

2.19. In vitro kinase assay of DGKζ

The DGKζ activity was detected by an ADP-Glo™ kinase assay kit (V9101, Promega, Madison, WI, USA). 6 × His-tagged,

1 cells were transfected with siNC or si*DGKZ*, followed by LPS stimulation for 4 h. The IL-1β expression was detected by Q-PCR and Western blotting. (F−H) BMDMs from wild-type (WT) and *Dgkz*$^{-/-}$ mice were stimulated with LPS + ATP. The culture medium (CM) was collected for examination of IL-1β concentration (F) by HTRF, and added to the primary hepatocytes along with D-GalN. The levels of cleaved-PARP (c-PARP) and cleaved-Caspase 3 (c-Caspase 3) (G), and the activity of Caspase 3 (scar bar: 100 μm) (H) were determined. (I, J) ALF was induced in mice by LPS + D-GalN. After 1.5, 3 and 4 h, the protein level of DGKζ in the liver was determined by Western blotting (I). After 6 h, the protein levels of DGKζ in F4/80$^+$ and Ly6G$^+$ cells sorted from the liver were determined by Western blotting (J). (K) Hepatic DGKζ$^+$CD68$^+$ cells in Healthy Controls ($n = 6$) and ACLF patients ($n = 5$) were marked (scar bar: 50 μm) and counted. (L−N) WT and *Dgkz*$^{-/-}$ mice were administered with LPS + D-GalN for 6 h. The liver index (L), the levels of ALT, AST and LDH in plasma (M), the histological alterations of the liver (scar bar: 50 μm) (N), the frequency of MoMFs in liver (O), the mRNA level of *Il1b* in liver (P), and the IL-1β concentration in plasma (Q) were evaluated. Data are displayed as mean ± SEM (For A−H, $n = 3$; For I, J, I−N, $n = 6$). *$P < 0.05$, **$P < 0.01$ *vs*. the indicated group.

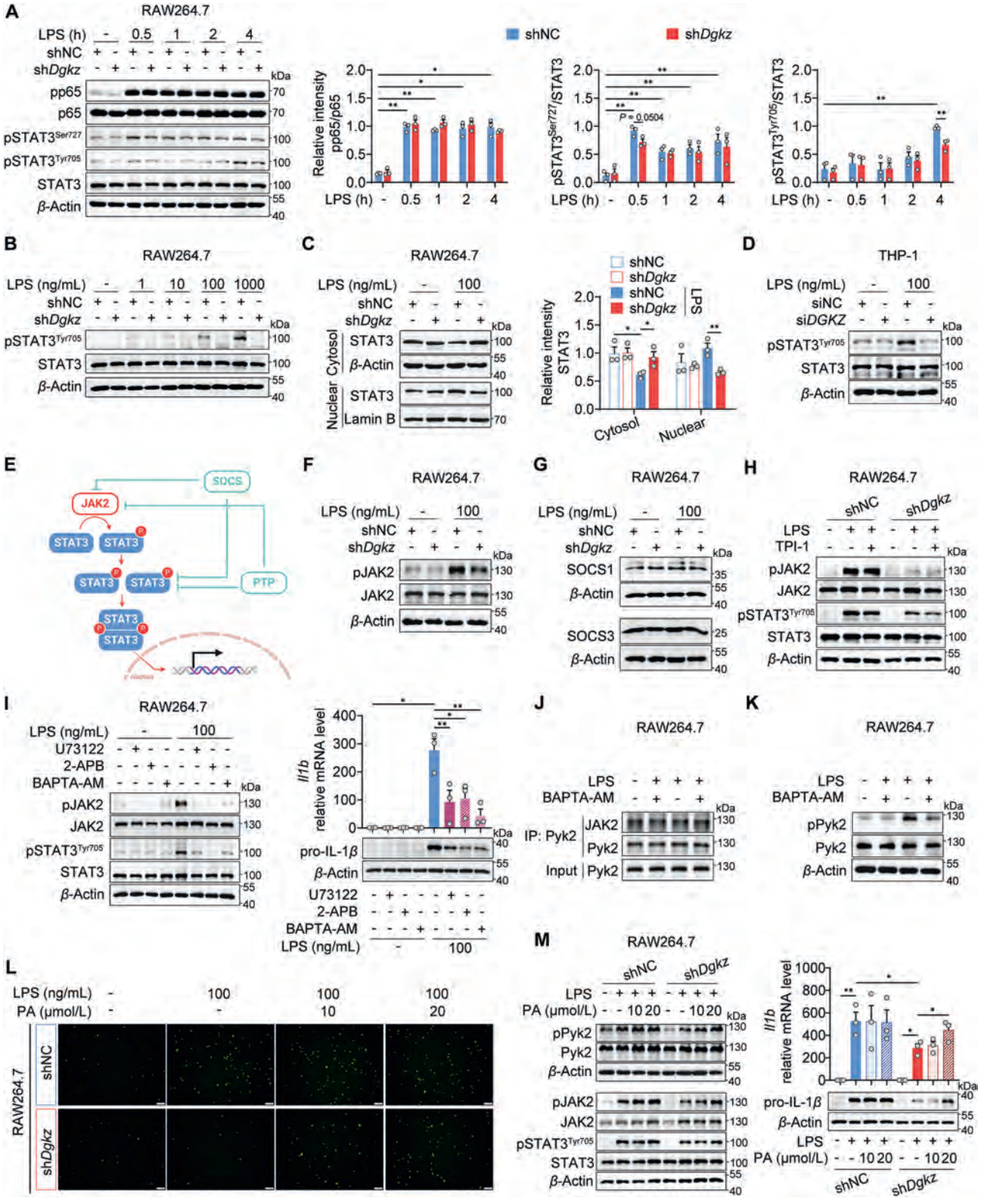

Figure 5 DGKζ−STAT3 axis drives IL-1β production in macrophages. (A−C) Stable shNC- and sh*Dgkz*-RAW264.7 cells were stimulated with LPS for the indicated time. The levels of pp65, pSTAT3^{Ser727}, and pSTAT3^{Tyr705}, as well as the nuclear translocation of STAT3 were determined by Western blotting. (D) PMA-differentiated THP-1 cells were transfected with siNC or si*DGKZ*, followed by LPS stimulation for 4 h. The level of pSTAT3^{Tyr705} was determined by Western blotting. (E) Regulators of the JAK2−STAT3 pathway (created with Biorender.com). (F, G) Stable shNC- and sh*Dgkz*-RAW264.7 cells were stimulated with LPS for 4 h. The levels of pJAK2 (F), SOCS1, and SOCS3 (G) were determined by Western blotting. (H) Stable shNC- and sh*Dgkz*-RAW264.7 cells (with or without TPI-1 (3 μmol/L) pretreatment for 30 min) were stimulated with LPS for 4 h. The levels of pJAK2 and pSTAT3^{Tyr705} were determined by Western blotting. (I) RAW264.7 cells (with or without U73122

recombinant full-length human DGKζ was used as the enzyme. 1,2-Dioleoyl-*sn*-glycerol (0.28 mmol/L; D0138, Sigma−Aldrich), reconstituted in octyl-β-D-glucopyranoside (200 mmol/L; HY-116285, MedChemExpress) micelles, was used as the substrate mixed with ATP. Both the enzyme and substrate−ATP mixture were diluted in assay buffer (50 mmol/L MOPS, 1 mmol/L DTT, 100 mmol/L NaCl, 10 mmol/L $MgCl_2$, 1 μmol/L $CaCl_2$). The assay was carried out in a volume of 5 μL comprising 1 μL CAM12203/BAY 2965501, 1 μL enzyme solution (final concentration: 8 nmol/L), together with 3 μL substrate (final concentration: 3.2 μmol/L)−ATP (final concentration: 60 μmol/L) mixture.

2.20. ALF induction and treatments

For the LPS + D-GalN-induced model, two experimental approaches including preventive and therapeutic administration were applied. In the case of preventive administration, mice were i.p. injected with CAM12203 or BAY 2965501 once a day for 3 days, and subjected to LPS (10 μg/kg) + D-GalN (400 mg/kg) 15 min after the last dosing. In the case of therapeutic administration, CAM12203 was administered (i.p.) 1 h after the injection of LPS + D-GalN. After 6 h, blood was collected from the eye sockets of mice for biochemistry assay, and the mice were euthanized for further analysis.

2.21. Liver processing for flow cytometry and cell isolation

The livers were chopped into pieces, digested in DMEM with collagenase (0.25 mg/mL; C5138, Sigma−Aldrich) for 30 min (37 °C), and filtered (70 μm). After red blood cells were removed by lysis buffer (C3702, Beyotime), the remaining cells were either stained with PE/Cyanine7 anti-mouse CD45 (103113, BioLegend, San Diego, CA, USA), FITC anti-mouse/human CD11b (101205, BioLegend), and PE anti-mouse F4/80 (123109, BioLegend), followed by flow cytometric measurement, or subjected to sorting by anti-F4/80 microBeads (130-110-443, Miltenyi, Bergisch-Gladbach, Germany).

2.22. Histological analysis and immunostaining

Liver tissue fixed in paraformaldehyde was desiccated and embedded before being cut into sections. For histological analysis, hematoxylin and eosin (H&E) were used to stain the sections. For immunofluorescence staining, the sections were processed for heat-induced epitope retrieval, followed by incubation with 5% BSA as well as 0.1% Triton X-100 for 1 h (room temperature). Subsequently, the sections were probed with a mixture of Rabbit anti-DGKζ antibody (1:200; ab239081, Abcam) and Mouse anti-CD68 antibody (1:200; abs158352, Absin, Shanghai, China) overnight (4 °C). After being washed, a mixture of relevant fluorescence-labeled secondary antibodies was added for an 1 h-incubation (room temperature). Finally, the sections were stained for 10−15 min with DAPI (1:1000; C1002, Beyotime), and mounted with antifade medium (P0126, Beyotime). For immunohistochemistry staining, the sections were antigen-retrieved, and treated for 30 min with 3% H_2O_2. After being blocked, the sections were subjected to rabbit anti-CD68 antibody (1:1000; ab125212, Abcam) or rat anti-F4/80 antibody (1:500; sc-71085, Santa Cruz, Santa Cruz, CA, USA), followed by peroxidase-conjugated secondary antibodies and DAB. Then, the sections were processed by hematoxylin, dehydrated, and mounted.

2.23. Statistical analysis

Data analyzed by SPSS 22 are displayed by mean ± standard error of mean (SEM). Student's *t* test was performed to compare the differences between two groups. According to the homogeneity test of variance, One-way ANOVA followed by LSD or Games−Howell test was carried out to evaluate the differences among multiple groups. $P < 0.05$ was statistically significant.

3. Results

3.1. CAM12203 suppresses macrophage-mediated inflammation to alleviate secondary hepatocyte damage

To confirm the anti-inflammatory effect of CAM12203 (Fig. 1A), its cytotoxicity was first evaluated by CCK-8. The cell viabilities of RAW264.7 cells (a mouse macrophage cell line), PMA-differentiated THP-1 cells (a human macrophage cell line), and BMDMs (primary mouse macrophages) remained unaltered when treated with the compound at 2.5, 5, 10, and 20 μmol/L (Supporting Information Fig. S1). However, CAM12203 (2.5, 5, 10, and 20 μmol/L) possessed a concentration-dependent down-regulation of the mRNA levels of *Tnfa*, *Il6*, *Il1b* and *Mcp1* in LPS-stimulated RAW264.7 cells, with the most significant impact observed on *Il1b* (Fig. 1B). The inhibitory effects of CAM12203 on the mRNA level of *IL1B* in THP-1 cells and *Il1b* in BMDMs, and the protein level of pro-IL-1β in all cell types were further elucidated (Fig. 1C and D). Additionally, IL-1β secretion from LPS + ATP-stimulated BMDMs was reduced by CAM12203 (5, 10, and 20 μmol/L) (Fig. 1E).

The CM of BMDMs was collected and added to primary hepatocytes along with D-GalN (Fig. 1F), so as to induce cell damage indicated by the increased cleavage levels of apoptosis-relevant proteins such as PARP and Caspase 3 and the enhanced activity of Caspase 3. As shown in Fig. 1G and H, the supernatant of LPS + ATP-stimulated BMDMs (without CAM12203 pre-treatment) clearly exacerbated hepatocyte damage compared to that of unstimulated BMDMs, whereas hepatocytes incubated with CAM12203-pretreated BMDMs-CM exhibited an improved condition. To assess the direct effect of CAM12203 on hepatocytes, the compound was dissolved in the supernatant of LPS + ATP-stimulated BMDMs, and added to primary hepatocytes along with D-GalN. The hepatocytes still suffered apoptosis, eliminating the

(10 μmol/L), 2-APB (50 μmol/L), and BAPTM-AM (10 μmol/L) pretreatment for 30 min) were stimulated with LPS for 4 h. The levels of pJAK2 and $pSTAT3^{Tyr705}$ as well as IL-1β expression were determined by Western blotting and Q-PCR. (J, K) RAW264.7 cells (with or without BAPTM-AM (10 μmol/L) pretreatment for 30 min) were stimulated with LPS for 4 h. The binding between Pyk2 and JAK2 (J) was examined by immunoprecipitation, and the levels of pPyk2 and pJAK2 (K) were determined by Western blotting. (L, M) Stable shNC- and sh*Dgkz*-RAW264.7 cells were stimulated with LPS as well as PA for 4 h. The concentration of Ca^{2+} (L) was measured by Fluo-4 AM (scar bar: 50 μm). The levels of pPyk2, pJAK2, and $pSTAT3^{Tyr705}$ as well as IL-1β expression (M) were determined by Western blotting and Q-PCR. Data are displayed as mean ± SEM ($n = 3$). *$P < 0.05$, **$P < 0.01$ *vs*. the indicated group.

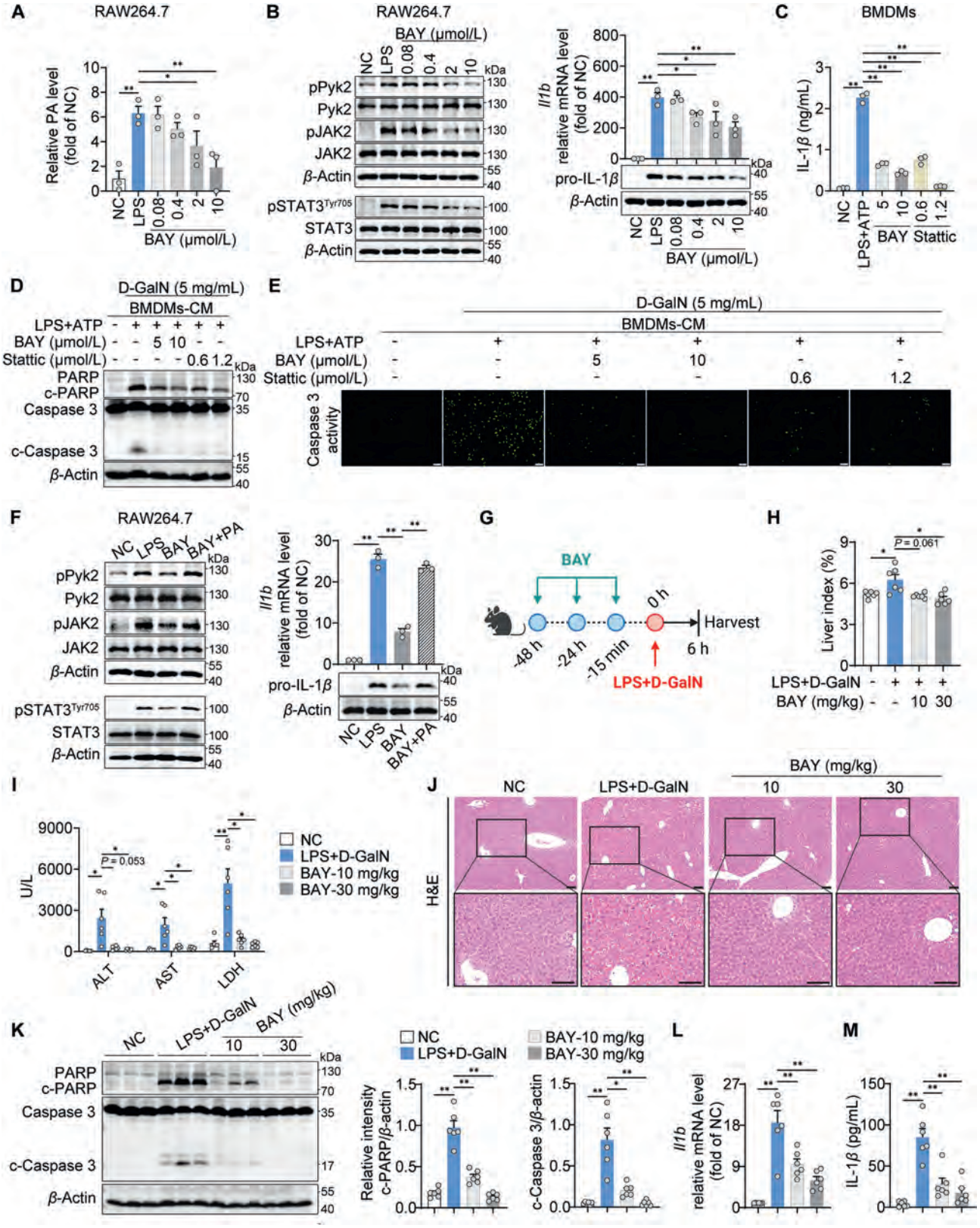

Figure 6 BAY 2965501 (BAY) ameliorates macrophage-mediated inflammation and liver failure. (A) RAW264.7 cells (with or without BAY pretreatment for 2 h) were stimulated with LPS for 0.25 h. The level of PA was measured by a commercial kit. (B) RAW264.7 cells (with or without BAY pretreatment for 2 h) were stimulated with LPS for 4 h. The levels of pPyk2, pJAK2, and pSTAT3^{Tyr705} as well as IL-1β expression were determined by Western blotting and Q-PCR. (C−E) BMDMs (with or without BAY/Stattic pretreatment for 2 h) were stimulated with LPS (4 h) + ATP (another 45 min). The culture medium (CM) was collected for examination of IL-1β concentration (C) by HTRF, and added to the

direct hepatoprotective effect of CAM12203 (Fig. 1I and J). These results suggest that CAM12203 suppresses macrophage-mediated inflammation to alleviate secondary hepatocyte damage.

3.2. CAM12203 exerts an ameliorative effect on acute liver failure in mice

To evaluate the *in vivo* efficacy of CAM12203, a model of ALF induced by LPS in combination with D-GalN was established, and CAM12203 was administered according to a preventive treatment protocol (Fig. 2A). The results showed that, by contrast with the model group without CAM12203 pretreatment, in which severe liver injury emerged 6 h after LPS + D-GalN injection, CAM12203 (10 and 30 mg/kg) group manifested a remarkable reduction of liver index, down-regulation of liver function reflected by plasma ALT, AST and LDH levels, as well as attenuation of pathological alterations and cleavage rates of apoptotic markers PARP and Caspase 3 in liver (Fig. 2B−E), signifying a great disease remission attributed to CAM12203. The inflammatory responses elicited by LPS + D-GalN in mice were also largely suppressed, as evidenced by a reduced quantity of hepatic $CD68^+$ and $F4/80^+$ macrophages (Fig. 2F), along with diminished IL-1β levels in both liver tissue and plasma (Fig. 2G and H). Moreover, following an alternative protocol, the therapeutic administration of CAM12203 (30 mg/kg) still yielded inhibitory effects on disease symptoms and inflammatory stress (Supporting Information Fig. S2), further substantiating its efficacy in protecting against ALF.

Clodronate liposomes (CL), a classical agent used for macrophage depletion, was proved efficient in our study, as the frequencies of both the KCs (identified as $F4/80^{hi}CD11b^{lo}$ cells) and MoMFs (identified as $F4/80^{lo}CD11b^{hi}$ cells)[29] in liver $CD45^+$ cell population were decreased (Fig. 2I). Of note, except a slight increase in LDH level probably due to macrophage apoptosis (LDH is not an indicator of hepatocyte-specific damage, unlike ALT and AST), the LPS + D-GalN-induced symptoms were markedly alleviated in CL-treated group (Fig. 2J−L), consistent with the previous finding that highlight the crucial involvement of macrophages in the pathogenesis of ALF[12]. However, when macrophages were depleted, CAM12203 (10 mg/kg) no longer restrained ALF progression, as the liver index, the liver function, and histological state remained unchanged (Fig. 2J−L). These results suggest that CAM12203 exerts an ameliorative effect on ALF in mice by limiting macrophage-mediated inflammation.

3.3. DGKζ is identified as a potential target of CAM12203

To identify the direct molecular target of CAM12203 and elucidate the mechanisms underlying its anti-inflammatory effect, affinity-based protein profiling[30,31], a chemical proteomics strategy, was employed. Based on our previous findings that the introduction of an acrylate group on the western phenyl ring has a decisive impact on anti-inflammatory activity, the synthesis of the active probe retained this structural unit, while a biotin moiety was introduced on the opposite side to facilitate the labeling of target protein (Fig. 3A). As revealed in Fig. 3B and C, the biotinylated probe of CAM12203 (10 and 20 μmol/L) retained the ability to decrease IL-1β expression and secretion in LPS-stimulated RAW264.7 cells and LPS + ATP-stimulated BMDMs. Thus, the probe could be applied for subsequent experiments.

According to the scheme, RAW264.7 lysates were pre-incubated with or without CAM12203, followed by the treatment with the biotinylated probe. After streptavidin enrichment, in-gel digestion, and LC−MS/MS analysis, the binding proteins were obtained and quantified (Fig. 3D). A total of 96 proteins pulled down by the probe (10 μmol/L) were competed with an excess amount of CAM12203 (300 μmol/L) (Supporting Information Table S2 and Fig. 3E), thereby being identified as the potential targets. Among these proteins, compelling evidence suggests a close linkage between DGKζ and immune cell functions[32]. Therefore, it is speculated that DGKζ might serve as a cellular target of CAM12203 to regulate macrophage-mediated inflammatory responses. The results of Western blotting assay using a specific antibody against DGKζ further confirmed that DGKζ was pulled down by the probe (10 μmol/L) from RAW264.7 lysates, and the binding was blocked by preincubating with CAM12203 (300 μmol/L) (Fig. 3F). Meanwhile, DARTS experiment demonstrated that CAM12203 (2.5, 5, 10, and 20 μmol/L) stabilized DGKζ in RAW264.7 cells by increasing resistance to proteolysis (Fig. 3G). CETSA revealed that CAM12203 (10 μmol/L) enhanced the thermal stability of both mouse and human DGKζ in RAW264.7 and HEK293T cells, respectively (Fig. 3H and Supporting Information Fig. S3). However, weaker or no effect could be observed on other members of the DGK family, including DGKα, DGKγ, DGKδ, DGKε, and DGKθ (Fig. S3). In addition, the SPR assay revealed that the K_D value of CAM12203 was 6.33 μmol/L (Fig. 3I). These results collectively indicate the direct binding between CAM12203 and DGKζ.

3.4. DGKζ is involved in macrophage-mediated inflammation and liver failure

Based on the aforementioned data, the role of DGKζ in macrophage-mediated inflammation was comprehensively investigated. The results demonstrated that LPS triggered a time- and concentration-reliant elevation in the levels of DGKζ and its downstream product PA in RAW264.7 cells (Fig. 4A and B). Knockdown of DGKζ by shRNA counteracted the increasing effect of LPS on PA, suggesting that the induction of PA was at least partially attributed to DGKζ (Fig. 4B and Supporting Information Fig. S4A). In particular, LPS boosted DGKζ-derived PA within 0.25 h, despite the longer duration required for the up-regulation of DGKζ protein, indicating that aside from the protein level, LPS could stimulate DGKζ activity to some extent (Fig. 4A and B). Moreover, knockdown of DGKζ significantly suppressed IL-1β expression in LPS-stimulated RAW264.7 cells (Fig. 4C and D).

primary hepatocytes along with D-GalN. The levels of cleaved-PARP (c-PARP) and cleaved-Caspase 3 (c-Caspase 3) (D), and the activity of Caspase 3 (scar bar: 100 μm) (E) were determined. (F) RAW264.7 cells were pretreated with or without BAY for 2 h, and stimulated with LPS as well as PA for 4 h. The levels of pPyk2, pJAK2, and $pSTAT3^{Tyr705}$ as well as IL-1β expression were determined by Western blotting and Q-PCR. (G) Overall scheme of the preventive administration study for BAY (created with Biorender.com). (H−M) The liver index (H), the levels of ALT, AST and LDH in plasma (I), the histological alterations of the liver (scar bar: 100 μm) (J), the protein levels of c-PARP and c-Caspase 3 in liver (K), the mRNA level of *Il1b* in liver (L), and the IL-1β concentration in plasma (M) were evaluated. Data are displayed as mean ± SEM (For A−F, $n = 3$; For H−M, $n = 6$). *$P < 0.05$, **$P < 0.01$ *vs*. the indicated group.

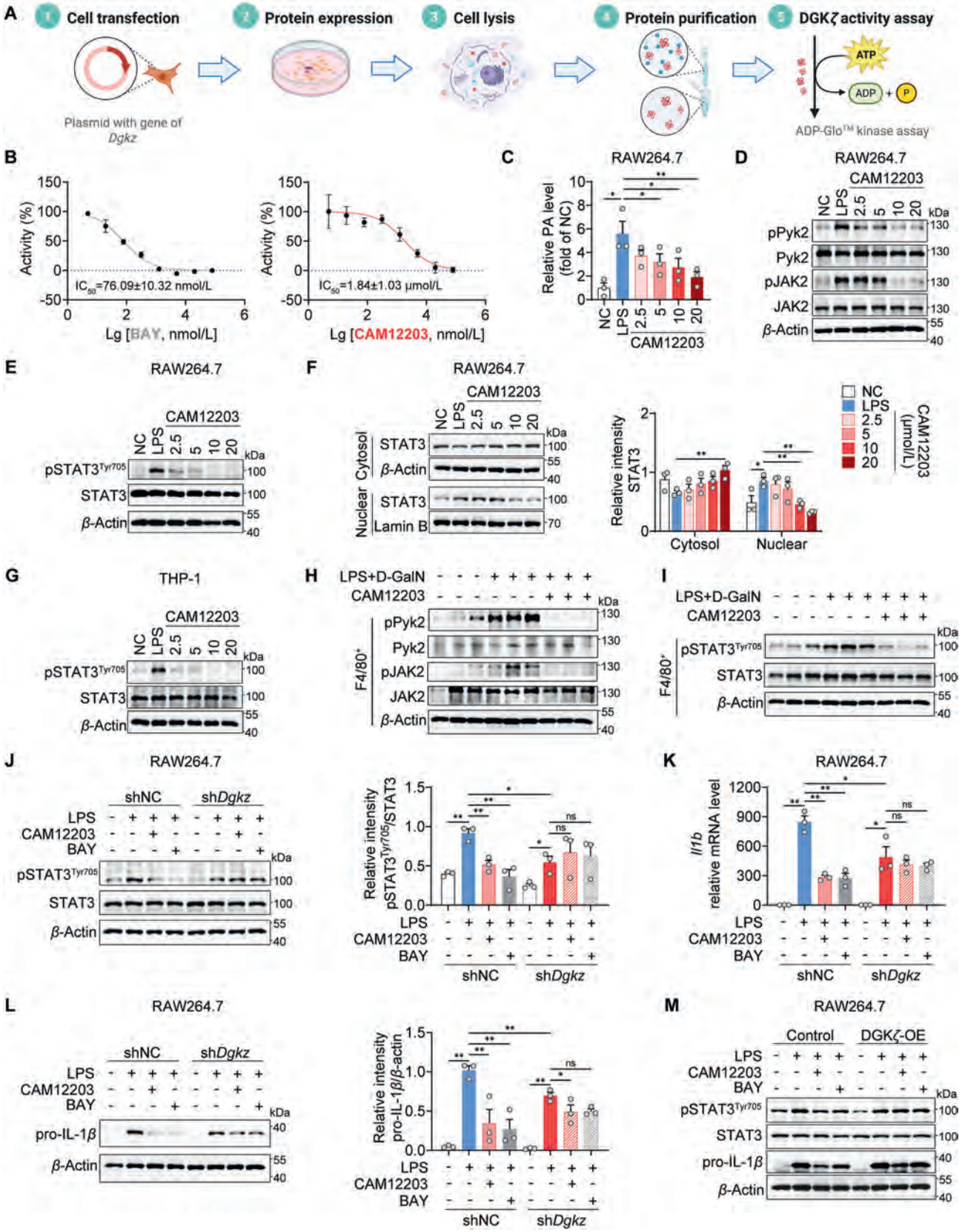

Figure 7 The anti-inflammatory effect of CAM12203 relies on DGKζ. (A) Overall scheme of the examination of DGKζ activity (created with Biorender.com). (B) The effects of BAY 2965501 (BAY) and CAM12203 on DGKζ activity were measured. (C) RAW264.7 cells (with or without CAM12203 pretreatment for 2 h) were stimulated with LPS for 0.25 h. The level of PA was measured by a commercial kit. (D−F) RAW264.7 cells (with or without CAM12203 pretreatment for 2 h) were stimulated with LPS for 4 h. The levels of pPyk2, pJAK2 (D) and

Transient transfection with siRNA diminished DGKζ level as well (Fig. S4B), and its suppressive impact on IL-1β expression was also been observed in LPS-stimulated THP-1 cells (Fig. 4E), while DGKζ-deficient BMDMs from DGKζ knockout (*Dgkz*$^{-/-}$) mice lost the ability to produce IL-1β upon LPS + ATP stimulation and failed to induce hepatocyte damage (Fig. S4C and S4D, Fig. 4F−H).

In vivo, LPS + D-GalN up-regulated DGKζ level in the liver in a time-reliant manner (Fig. 4I). Specifically, there was an elevation in the amount of DGKζ in macrophages isolated from the liver of ALF mice using F4/80 microbeads (Fig. 4J). A noticeable but less pronounced increase was observed in the amount of DGKζ in Ly6G^{+} neutrophils (Fig. 4J). Immunofluorescence staining revealed that, the quantity of DGKζ^{+}CD68^{+} cells in ACLF patients, who suffered ALF with known liver diseases, was greater than that in the healthy control group (Fig. 4K). Of note, *Dgkz*$^{-/-}$ mice were refractory to ALF induction, as evidenced by limited liver index, plasma ALT, AST and LDH levels, histological alterations and frequency of infiltrated macrophages (MoMFs) in liver, as well as IL-1β levels in both liver tissue and plasma (Fig. 4L−Q). These findings suggest that DGKζ is instrumental for macrophage-mediated inflammation and liver failure.

3.5. DGKζ drives IL-1β production in macrophages via its kinase activity and subsequent STAT3 activation

To explore the mechanism by which DGKζ regulated macrophages, its effects on NF-κB and STAT3, which are crucial pathways involved in IL-1β transcription[10,33,34], were assessed. The findings demonstrated that the knockdown of DGKζ in RAW264.7 cells markedly inhibited LPS-induced classical activation of STAT3 (phosphorylation at Tyr705), while showing a weaker impact on nonclassical activation of STAT3 (phosphorylation at Ser727) and no effect on NF-κB activation (phosphorylation of p65) (Fig. 5A and B). Consistently, LPS-induced nuclear translocation of STAT3, which follows the phosphorylation at Tyr705 residue, was suppressed by sh*Dgkz* (Fig. 5C), and the inhibitory effect of si*DGKZ* on pSTAT3^{Tyr705} was confirmed in LPS-stimulated THP-1 cells (Fig. 5D).

To illustrate how DGKζ controlled the classical STAT3 activation, the involvement of upstream regulators of STAT3 was evaluated. As shown in Fig. 5E, JAK2 serves as a traditional positive regulator, while SOCS proteins and protein tyrosine phosphatases exert negative regulation on the JAK2−STAT3 cascade[35]. The data revealed that, the phosphorylation of JAK2 was restricted in sh*Dgkz*-RAW264.7 cells (Fig. 5F). Nevertheless, the expression of SOCS1/3 remained unaltered (Fig. 5G), and the inhibition of JAK2−STAT3 resulting from DGKζ knockdown could not be attenuated by TPI-1 (Fig. 5H), an inhibitor of Src homology region 2 domain-containing phosphatase-1 (SHP-1) which belongs to protein tyrosine phosphatases.

It has been reported that Pyk2, a calcium-dependent tyrosine kinase, binds to JAK2 in resting vascular smooth muscle cells, and the latter is activated by increased Ca^{2+} concentration upon stimulation with calcium ionophore A23187 or angiotensin II[36,37]; Pyk2 kinase-inactive mutant or Pyk2 phosphorylation site mutant disrupts angiotensin II-induced JAK2 phosphorylation[36]; U73122, an inhibitor targeting phospholipase C (PLC), blocks IL-1β production induced by LPS in dU937 cells and primary peritoneal macrophages[38], implying a connection between PLC−inositol 1,4,5-trisphosphate (IP_3)−Ca^{2+} signaling and JAK2−STAT3 cascade as well as subsequent IL-1β production. On the other hand, a connection between DGKζ and PLC−IP_3−Ca^{2+} signaling exists as well: DGKζ metabolite PA allosterically activates PLCγ, and induces the production of PLC substrate phosphatidylinositol 4,5-bisphosphate (PIP_2)[39,40]; DGKζ knockout leads to decreased PLCγ activity and Ca^{2+} responses in mast cells[41]. Therefore, we hypothesized that PLC−IP_3−Ca^{2+} signaling linked DGKζ to JAK2−STAT3 cascade in macrophages. To validate the hypothesis, the inhibitors targeting each step within PLC−IP_3−Ca^{2+} signaling were used. As revealed in Fig. 5I, in addition to U73122, both IP_3R inhibitor 2-APB and Ca^{2+} chelators BAPTA-AM significantly restricted the phosphorylation of JAK2 and STAT3, along with the mRNA level of *Il1b* and protein level of pro-IL-1β in LPS-stimulated RAW264.7 cells. Immunoprecipitation experiments demonstrated the association between Pyk2 and JAK2 in resting macrophages, although a stronger effect was not observed upon LPS treatment (Fig. 5J). Meanwhile, LPS induced Ca^{2+}-dependent activation of Pyk2, as the phosphorylation of the protein was enhanced, and the effect was blocked by BAPTA-AM (Fig. 5K). Furthermore, knockdown of DGKζ caused a decrease in Ca^{2+} level and Pyk2 phosphorylation, with parallel reduction in JAK2−STAT3 activation and IL-1β production, the effects of which could be almost reversed by exogenous PA supplementation (Fig. 5L and M). These data indicate that DGKζ drives IL-1β production in macrophages *via* its kinase activity and subsequent STAT3 activation.

3.6. A clinical-stage DGKζ inhibitor ameliorates macrophage-mediated inflammation and liver failure

Then, a clinical-stage DGKζ inhibitor named BAY 2965501[42] was used as the tool drug to further validate the mechanism of DGKζ and the feasibility of the DGKζ targeting strategy for macrophage-mediated inflammation and liver failure. As shown in Fig. 6A, BAY 2965501 (0.08, 0.4, 2, and 10 μmol/L) exhibited a concentration-dependent reduction in cellular PA level in LPS-stimulated RAW264.7 cells. The downstream phosphorylation of Pyk2, JAK2 and STAT3, as well as the expression of IL-1β were also decreased by BAY 2965501 (0.4, 2, and 10 μmol/L) (Fig. 6B). Moreover, BAY 2965501 (5 and 10 μmol/L) significantly restricted IL-1β secretion in LPS + ATP-stimulated BMDMs, and a similar effect caused by Stattic (0.6 and 1.2 μmol/L), a specific

pSTAT3^{Tyr705} (E), and the cytosol as well as nuclear levels of STAT3 (F) were determined by Western blotting. (G) PMA-differentiated THP-1 cells (with or without CAM12203 pretreatment for 2 h) were stimulated with LPS for 4 h. The level of pSTAT3^{Tyr705} was determined by Western blotting. (H, I) Mice were administered by CAM12203 (30 mg/kg), and ALF was induced by LPS + D-GalN. After 6 h, the levels of pPyk2, pJAK2 (H), and pSTAT3^{Tyr705} (I) in F4/80^{+} cells sorted from the liver were determined by Western blotting. (J−L) Stable shNC- and sh*Dgkz*-RAW264.7 cells (with or without CAM12203/BAY pretreatment for 2 h) were stimulated with LPS for 4 h. The level of pSTAT3^{Tyr705} and IL-1β expression were determined by Western blotting and Q-PCR. (M) RAW264.7 cells were transfected with Control or DGKζ-OE plasmid, and treated with or without CAM12203/BAY for 2 h, followed by LPS simulation for 4 h. The levels of pSTAT3^{Tyr705} and pro-IL-1β were determined by Western blotting. Data are displayed as mean ± SEM ($n = 3$). *$P < 0.05$, **$P < 0.01$ *vs*. the indicated group; ns, not significant.

inhibitor of STAT3, could be observed (Fig. 6C). Compared to the control group, neither BAY 2965501- nor Stattic-pretreated BMDMs remained the ability to induce hepatocyte damage, which underscored the inhibitory impact of these compounds on macrophage-mediated inflammatory responses (Fig. 6D and E). The data in Fig. 6F show that, when supplemented with PA, BAY 2965501 (10 μmol/L) failed to down-regulate the phosphorylation of Pyk2, JAK2, and STAT3 as well as the expression of IL-1β in LPS-stimulated RAW264.7 cells, thereby confirming the pivotal role of DGKζ activity in macrophage-mediated inflammation.

In vivo, the ALF model induced by LPS + D-GalN was replicated. The results demonstrated that preventively i.p. administered BAY 2965501 (10 and 30 mg/kg) significantly alleviated the disease symptoms, as evidenced by the limited liver index, plasma ALT, AST, and LDH levels, pathological alterations, cleaved-PARP, and cleaved-Caspase 3 levels in liver (Fig. 6G−K). What's more, BAY 2965501 (10 and 30 mg/kg) resulted in a notable decrease in IL-1β levels in both liver tissue and plasma (Fig. 6L and M). Following the therapeutic treatment protocol, there was a tendency towards a lower liver index in mice injected with BAY 2965501 (30 mg/kg), and the DGKζ inhibitor exerted obvious ameliorative effects on other liver symptoms as well as inflammation caused by LPS + D-GalN (Supporting Information Fig. S5). These findings indicate that BAY 2965501 attenuates STAT3 signaling downstream of DGKζ to mitigate macrophage-mediated inflammation and liver failure.

3.7. CAM12203 is a new DGKζ inhibitor

To evaluate the inhibitory potential of CAM12203 on the kinase activity of DGKζ, recombinant human DGKζ was expressed in HEK293T cells, followed by protein purification, and its activity was tested by ADP-Glo assay (Fig. 7A). The IC_{50} value for BAY 2965501 was determined to be 76.09 nmol/L (Fig. 7B), suggesting the successful establishment of the detection system, while the IC_{50} value for CAM12203 was 1.84 μmol/L (Fig. 7B). At the cellular level, it was observed that CAM12203 (2.5, 5, 10, and 20 μmol/L) concentration-dependently down-regulated the downstream signals of DGKζ in LPS-stimulated RAW264.7 cells, including the PA level, the phosphorylation of Pyk2, JAK2 and STAT3, as well as the nuclear translocation of STAT3 (Fig. 7C−F). CAM12203 also restricted STAT3 phosphorylation in LPS-stimulated THP-1 cells at concentrations of 2.5, 5, 10, and 20 μmol/L (Fig. 7G), and limited the levels of pPyk2, pJAK2 and $pSTAT3^{Tyr705}$ in $F4/80^{+}$ macrophages sorted from the mice administered by LPS+D-GalN with a dosage of 30 mg/kg (Fig. 7H and I).

When DGKζ was knocked down by shRNA, the inhibitory impact of CAM12203 (10 μmol/L) on STAT3 activation and IL-1β production disappeared, and a similar pattern existed in terms of the positive control BAY 2965501 (10 μmol/L) (Fig. 7J−L). Overexpression of DGKζ counteracted the anti-inflammatory effects of CAM12203 (10 μmol/L) and BAY 2965501 (10 μmol/L) (Fig. S4E and Fig. 7M), further uncovering the reliance on DGKζ. These results indicate that besides BAY 2965501, CAM12203 is a new DGKζ inhibitor.

4. Discussion

Till now, a growing body of natural products has been extensively explored for their therapeutic potential against a variety of diseases. Nevertheless, the journey from the discovery to the approval and application of these natural products as novel drugs is both time-consuming and expensive. This is partially attributed to the challenges associated with comprehending their action mode, in which the target identification is the crucial step. The burgeoning discipline of chemical proteomics has witnessed a recent increase in its application for the target identification of drugs and other bioactive small molecules[43,44]. In this study, on the basis of clarifying that CAM12203, a derivative of XN, exerted inhibitory effects on ALF by restricting macrophage-mediated inflammation, we attempted to explore its target protein through chemical proteomics. By synthesizing the biotinylated probe that retained the bioactivities and taking advantage of its high affinity to streptavidin, the potential target proteins were obtained and identified through high-resolution detection methods such as MS. Among them, DGKζ caught our eyes owing to its role in immune cells, and we further confirmed the binding between CAM12203 and DGKζ through DARTS and CETSA.

Indeed, only recently has DGKζ been established as a key component of immune cell regulation: In T cells, DGKζ deletion exerts a heightened reactivity to T-cell receptor stimulation, while DGKζ promotes T cell anergic responses and Th1 differentiation[45−48]. In mast cells, DGKζ takes control over FcεRI-mediated degranulation, and knockout of DGKζ causes weakened local allergic reactions[41]. In dendritic cells, DGKζ deficiency leads to enhanced PI3K activity and diminished production of IL-12 p40 and TNF-α under the stimulation of LPS or soluble antigens of *Toxoplasma gondii*[49]. The association between DGKζ and macrophages has also been documented in a sheer volume of literatures. Compared to other members in the DGK family, DGKζ is the subtype expressed most abundantly in macrophages, suggesting a potential role it plays in macrophage-regulated responses[50,51]. Liu et al.[49] and Mahajan et al.[52] have noted that DGKζ knockout significantly attenuates the production of proinflammatory cytokines in LPS-stimulated BMDMs. Herein, we unveiled that LPS raised DGKζ level as well as its activity to a certain extent, and verified its regulatory effects on IL-1β transcription in three types of macrophage lines, including mouse/human cell lines and primary cells, through stable/transient transfection-mediated DGKζ knockdown and DGKζ knockout. Additionally, since macrophage-mediated inflammatory responses are key events in ALF development, it was speculated that DGKζ might be a driver of liver failure. The assumption was supported by determining the DGKζ level during liver failure progression, along with comparing the symptoms between wild-type and $Dgkz^{-/-}$ mice injected with LPS + D-GalN. However, the underlying mechanism by which DGKζ mediates the inflammatory responses, especially the transcription of IL-1β, remains unclear both domestically and internationally.

In macrophages, NF-κB and STAT3 are involved in the transcription of IL-1β. Upon stimulation, IκBα is phosphorylated by IKK and undergoes ubiquitin-dependent degradation, thereby leading to the phosphorylation and translocation of NF-κB heterodimer, p65/p50, into the nucleus where NF-κB serves as a transcription factor[53]. In terms of STAT3, both the non-classical and classical activation pathways mediate IL-1β transcription. On the one hand[38], LPS stimulation induces the formation of the TRAF6−TBK1−STAT3 complex, thus causing the phosphorylation of $STAT3^{Ser727}$. The phosphorylated STAT3 translocates into mitochondria, leading to the accumulation of succinate, an intermediate of the tricarboxylic acid cycle. In this non-classical activation pathway, since succinate can enhance the stability of hypoxia-inducible factor-1α (HIF-1α), the latter is a potential

mediator for succinate to regulate IL-1β transcription. On the other hand[34], in the classical activation pathway, JAK2 is activated, which phosphorylates STAT3 at Tyr705 residue. Subsequently, STAT3 dimerizes and translocates into the nucleus to regulate IL-1β transcription by itself[11,54]. We screened these pathways, and found that the JAK2−STAT3 cascade, namely the classical activation of the STAT3 pathway, contributes to the boosting effects of DGKζ on the transcription of IL-1β.

Moreover, given that DGKζ is a lipid-metabolizing kinase, it is of utmost necessity to focus on the participation of lipid metabolism in this inflammatory transcriptional system. Interestingly, activation of macrophages by Toll-like receptors (TLRs) rapidly alters their lipid metabolic programs, resulting in a model where lipid reprogramming is indispensable for ensuring appropriate function[55]. In line with this notion, chemical and genetic perturbation of TLR-mediated reprogramming of lipid homeostasis influences the capacity of macrophages to mediate inflammatory responses[55]. However, there is still a considerable gap in our understanding of the lipid composition that shapes the pro-inflammatory signals. A wealth of data has revealed that PA, the downstream product of DGKζ, serves as intermediates in the synthesis of all phospholipids, lipid bilayer constituents for modulating membrane fluidity, or signal transducers by associating with a variety of effector molecules, allowing it to govern diverse and vital biological events[56−58]. Among the PA-binding proteins, PLC has been reported to facilitate IL-1β production[38]. By converting membrane phospholipid, PIP_2, into IP_3, which binds to IP_3 receptors on the endoplasmic reticulum, PLC causes the release of Ca^{2+} into the cytoplasm[59]. A calcium-dependent tyrosine kinase, Pyk2, binds to JAK2 and regulates its activation in vascular smooth muscle cells[36,37], suggesting a linkage between PLC−IP_3−Ca^{2+} signaling and JAK2−STAT3 cascade in macrophages. Of note, kinetic analysis concludes that PA appears to activate PLCγ as an allosteric modifier[39], while another study discovers the role of DGKζ-generated PA in increasing PIP_2 production by stimulating the activity of phosphatidylinositol 4-phosphate 5-kinase Iα[40]. We therefore endeavored to explore whether and how PA produced by DGKζ signaled to the nucleus, and found that by favoring the activation of PLC−IP_3−Ca^{2+} signaling and subsequent JAK2−STAT3 cascade, DGKζ−PA axis drove IL-1β transcription in LPS-stimulated macrophages.

It should be mentioned that DGKζ is also a DAG-consuming enzyme, beyond its effect on PA generation. This means DGKζ acts as a molecular switch that simultaneously turns off DAG-regulated signals as well. However, the aspect regarding the role of DAG may be more complicated compared to that of PA in macrophages, as both DAG and PA levels are increased by inflammatory stimuli[60]. Yet the beneficial potential of DAG accumulation due to DGKζ limitation exists, as nonhydrolyzable DAG analogue PMA restricts the phosphorylation of $STAT3^{Tyr705}$ in LPS-treated BMDMs[52]. Despite the lack of investigation, it is conjectured that the increased DAG level can counteract PLC−IP_3−Ca^{2+}-mediated inflammatory responses unless it is promptly transformed into PA by DGKζ, since DAG is another product of PLC besides IP_3. This negative feedback regulation has been verified in airway smooth muscle cells, which indicates that DGKζ inhibition perturbs the DAG:PA ratio, thereby restricting Gq−PLC−IP_3−Ca^{2+}-mediated contractile signaling[61].

In this study, no matter what role DAG played, the essential involvement of PA reflected that DGKζ mediated IL-1β transcription through its kinase activity, and laid a theoretical foundation for the application of DGKζ inhibitors. To date, extensive efforts have been invested into the development of DGKζ inhibitors for cancer treatment. BAY 2965501, ASP1570, and BGB-30813 are three DGK inhibitors entering the clinical research stage. All of them are capable of restoring the DAG level in anergic T cells *via* DGKζ inhibition to facilitate T cell-mediated killing of tumor cells. Although the benefits of DGKζ inhibitors in tumor immunotherapy have been widely recognized, their effects on inflammation-related diseases such as ALF remain ambiguous. Our work is the first attempt to answer this question. As expected, we found that BAY 2965501 dampened the downstream signaling of DGKζ in LPS-stimulated macrophages, inhibited IL-1β production and subsequent hepatocyte apoptosis, thus leading to a great remission in LPS + D-GalN-injected mice. These results regarding the tool drug confirmed the mechanism by which DGKζ mediated inflammatory responses in macrophages and validated the feasibility of the DGKζ targeting strategy for liver failure. Notably, CAM12203 was proved to be a novel DGKζ inhibitor, as the molecular activity and downstream STAT3 pathway of DGKζ were attenuated by CAM12203, and the compound acted against inflammation in a DGKζ-dependent manner. This furnished us with confidence in the development of CAM12203 and other potential derivatives of XN as DGKζ inhibitors for ALF treatment.

5. Conclusions

We reveal that XN derivative CAM12203 inhibits IL-1β transcription in macrophages by binding to DGKζ and blocking the DGKζ−STAT3 axis, thereby exerting an ameliorative effect on ALF. This study is conducive to the development and application of CAM12203 or other potential derivatives, deepens the understanding of the pathological process of ALF, and offers DGKζ as a new therapeutic target for ALF.

Data availability

Upon reasonable request, source data are available from the corresponding author. All mass spectrometry raw data have been deposited to the iProX Consortium with Project ID: IPX0009841000 (URL: https://www.iprox.cn/page/project.html?id=IPX0009841000).

Acknowledgments

This work was supported by the National Science and Technology Major Project (2024ZD0523103, China), the National Natural Science Foundation of China (92457302; 82425058; 82304500; and 22494693), the National Key R&D Program of China (2020YFE0205600), the Yangfan Project of Shanghai Science and Technology Commission (23YF1456500, China), the Shanghai "Super Postdoctoral" Incentive Plan (2022692, China), the fellowship of China Postdoctoral Science Foundation (2023M733630), the Tian-Shan Talent Program (2022TSYCLJ0064, China), and the Youth Innovation Promotion Association of Chinese Academy of Sciences (E32R4001, China).

Author contributions

Yumeng Miao: Conceptualization, Data curation, Formal analysis, Funding acquisition, Investigation, Methodology, Writing-original draft preparation, Writing-review & editing. Tzuchun Lin: Conceptualization, Investigation, Methodology. Bianlin Wang: Investigation,

Methodology, Writing-original draft preparation. Junyu Xu: Investigation, Methodology, Writing-original draft preparation. Chongxian Li: Investigation, Methodology. Zuopeng Li: Investigation, Funding acquisition. Xinwen Zhang: Investigation. Chendong Zhou: Investigation. Tuerganaili Aji: Resources. Minjia Tan: Conceptualization, Writing-review & editing. Haji Akber Aisa: Conceptualization, Funding acquisition, Writing-review & editing. Jingya Li: Conceptualization, Funding acquisition, Project administration, Supervision, Writing-review & editing.

Conflicts of interest

The authors declare no conflict of interest.

Appendix A. Supporting information

Supporting information to this article can be found online at https://doi.org/10.1016/j.apsb.2025.06.019.

References

1. Rovegno M, Vera M, Ruiz A, Benítez C. Current concepts in acute liver failure. *Ann Hepatol* 2019;**18**:543−52.
2. Stravitz RT, Lee WM. Acute liver failure. *Lancet* 2019;**394**:869−81.
3. García-Cortés M, Ortega-Alonso A, Andrade RJ. Spanish group for the study of drug-induced liver disease (Grupo de Estudio para las Hepatopatías Asociadas a Medicamentos GEHAM). Safety of treating acute liver injury and failure. *Expet Opin Drug Saf* 2022;**21**:191−203.
4. Xu Y, Wang J, Ren H, Dai H, Zhou Y, Ren X, et al. Human endoderm stem cells reverse inflammation-related acute liver failure through cystatin SN-mediated inhibition of interferon signaling. *Cell Res* 2023;**33**:147−64.
5. Triantafyllou E, Woollard KJ, McPhail MJW, Antoniades CG, Possamai LA. The role of monocytes and macrophages in acute and acute-on-chronic liver failure. *Front Immunol* 2018;**9**:2948.
6. Roohani S, Tacke F. Liver injury and the macrophage issue: molecular and mechanistic facts and their clinical relevance. *Int J Mol Sci* 2021;**22**:7249.
7. Wen Y, Lambrecht J, Ju C, Tacke F. Hepatic macrophages in liver homeostasis and diseases-diversity, plasticity and therapeutic opportunities. *Cell Mol Immunol* 2021;**18**:45−56.
8. Zimmermann HW, Trautwein C, Tacke F. Functional role of monocytes and macrophages for the inflammatory response in acute liver injury. *Front Physiol* 2012;**3**:56.
9. Ilyas G, Zhao E, Liu K, Lin Y, Tesfa L, Tanaka KE, et al. Macrophage autophagy limits acute toxic liver injury in mice through down regulation of interleukin-1β. *J Hepatol* 2016;**64**:118−27.
10. Davis BK, Wen H, Ting JP. The inflammasome NLRs in immunity, inflammation, and associated diseases. *Annu Rev Immunol* 2011;**29**:707−35.
11. Samavati L, Rastogi R, Du W, Hüttemann M, Fite A, Franchi L. STAT3 tyrosine phosphorylation is critical for interleukin 1 beta and interleukin-6 production in response to lipopolysaccharide and live bacteria. *Mol Immunol* 2009;**46**:1867−77.
12. Zeng X, Liu G, Peng W, He J, Cai C, Xiong W, et al. Combined deficiency of SLAMF8 and SLAMF9 prevents endotoxin-induced liver inflammation by downregulating TLR4 expression on macrophages. *Cell Mol Immunol* 2020;**17**:153−62.
13. Qu XQ, Chen QF, Shi QQ, Luo QQ, Zheng SY, Li YH, et al. Hepatocyte-conditional knockout of phosphatidylethanolamine binding protein 4 aggravated LPS/D-GalN-induced acute liver injury *via* the TLR4/NF-κB pathway. *Front Immunol* 2022;**13**:901566.
14. Li S, Hu K, Li L, Shen Y, Huang J, Tang L, et al. Stattic alleviates acute hepatic damage induced by LPS/D-galactosamine in mice. *Innate Immun* 2021;**27**:201−9.
15. Zhang H, Ding F, Zhu Z, Sun Q, Yang C. Engineered ionizable lipid nanoparticles mediated efficient siRNA delivery to macrophages for anti-inflammatory treatment of acute liver injury. *Int J Pharm* 2023;**631**:122489.
16. Sultan M, Ben-Ari Z, Masoud R, Pappo O, Harats D, Kamari Y, et al. Interleukin-1α and Interleukin-1β play a central role in the pathogenesis of fulminant hepatic failure in mice. *PLoS One* 2017;**12**:e0184084.
17. Galli G, Saleh M. Immunometabolism of macrophages in bacterial infections. *Front Cell Infect Microbiol* 2021;**10**:607650.
18. Yan J, Horng T. Lipid metabolism in regulation of macrophage functions. *Trends Cell Biol* 2020;**30**:979−89.
19. York AG, Skadow MH, Oh J, Qu R, Zhou QD, Hsieh WY, et al. IL-10 constrains sphingolipid metabolism to limit inflammation. *Nature* 2024;**627**:628−35.
20. Spann NJ, Garmire LX, McDonald JG, Myers DS, Milne SB, Shibata N, et al. Regulated accumulation of desmosterol integrates macrophage lipid metabolism and inflammatory responses. *Cell* 2012;**151**:138−52.
21. Girisa S, Saikia Q, Bordoloi D, Banik K, Monisha J, Daimary UD, et al. Xanthohumol from hop: hope for cancer prevention and treatment. *IUBMB Life* 2021;**73**:1016−44.
22. Lupinacci E, Meijerink J, Vincken JP, Gabriele B, Gruppen H, Witkamp RF. Xanthohumol from hop (*Humulus lupulus* L.) is an efficient inhibitor of monocyte chemoattractant protein-1 and tumor necrosis factor-alpha release in LPS-stimulated RAW 264.7 mouse macrophages and U937 human monocytes. *J Agric Food Chem* 2009;**57**:7274−81.
23. Cho YC, Kim HJ, Kim YJ, Lee KY, Choi HJ, Lee IS, et al. Differential anti-inflammatory pathway by xanthohumol in IFN-γ and LPS-activated macrophages. *Int Immunopharmacol* 2008;**8**:567−73.
24. Cho JM, Yun SM, Choi YH, Heo J, Kim NJ, Kim SH, et al. Xanthohumol prevents dextran sulfate sodium-induced colitis *via* inhibition of IKKβ/NF-κB signaling in mice. *Oncotarget* 2017;**9**:866−80.
25. Lv H, Liu Q, Wen Z, Feng H, Deng X, Ci X. Xanthohumol ameliorates lipopolysaccharide (LPS)-induced acute lung injury *via* induction of AMPK/GSK3β−Nrf2 signal axis. *Redox Biol* 2017;**12**:311−24.
26. Ajiaikebaier D, Li Z, Lin T, Sun X, Wang B, Li J. Synthesis of pyranochalcone derivatives and their inhibitory effect on NF-κB activation. *Bioorg Med Chem Lett* 2021;**42**:128042.
27. Kong X, Liu W, Zhang X, Zhou C, Sun X, Cheng L, et al. HIF-1α inhibition in macrophages preserves acute liver failure by reducing IL-1β production. *FASEB J* 2023;**37**:e23140.
28. Li Y, Xu J, Lu Y, Bian H, Yang L, Wu H, et al. DRAK2 aggravates nonalcoholic fatty liver disease progression through SRSF6-associated RNA alternative splicing. *Cell Metab* 2021;**33**:2004−20.e9.
29. Yang Y, Ying G, Wu F, Chen Z. sTim-3 alleviates liver injury *via* regulation of the immunity microenvironment and autophagy. *Cell Death Discov* 2020;**6**:62.
30. Fang H, Peng B, Ong SY, Wu Q, Li L, Yao SQ. Recent advances in activity-based probes (ABPs) and affinity-based probes (AfBPs) for profiling of enzymes. *Chem Sci* 2021;**12**:8288−310.
31. Porta EOJ, Steel PG. Activity-based protein profiling: a graphical review. *Curr Res Pharmacol Drug Discov* 2023;**5**:100164.
32. Singh BK, Kambayashi T. The immunomodulatory functions of diacylglycerol Kinase ζ. *Front Cell Dev Biol* 2016;**4**:96.
33. Zhang Z, Li M, Tai Y, Xing Y, Zuo H, Jin X, et al. ZNF70 regulates IL-1β secretion of macrophages to promote the proliferation of HCT116 cells *via* activation of NLRP3 inflammasome and STAT3 pathway in colitis-associated colorectal cancer. *Cell Signal* 2024;**114**:110979.
34. Balic JJ, Albargy H, Luu K, Kirby FJ, Jayasekara WSN, Mansell F, et al. STAT3 serine phosphorylation is required for TLR4 metabolic reprogramming and IL-1β expression. *Nat Commun* 2020;**11**:3816.
35. Hu X, Li J, Fu M, Zhao X, Wang W. The JAK/STAT signaling pathway: from bench to clinic. *Signal Transduct Targeted Ther* 2021;**6**:402.
36. Frank GD, Saito S, Motley ED, Sasaki T, Ohba M, Kuroki T, et al. Requirement of Ca^{2+} and PKCδ for Janus kinase 2 activation by angiotensin II: involvement of PYK2. *Mol Endocrinol* 2002;**16**:367−77.

37. Garnovskaya MN, Mukhin YV, Turner JH, Vlasova TM, Ullian ME, Raymond JR. Mitogen-induced activation of Na^+/H^+ exchange in vascular smooth muscle cells involves janus kinase 2 and Ca^{2+}/calmodulin. *Biochemistry* 2003;**42**:7178−87.
38. Zhu L, Yuan C, Ma Y, Ding X, Zhu G, Zhu Q. Anti-inflammatory activities of phospholipase C inhibitor U73122: inhibition of monocyte-to-macrophage transformation and LPS-induced pro-inflammatory cytokine expression. *Int Immunopharmacol* 2015;**29**:622−7.
39. Jones GA, Carpenter G. The regulation of phospholipase C-gamma 1 by phosphatidic acid. Assessment of kinetic parameters. *J Biol Chem* 1993;**268**:20845−50.
40. Luo B, Prescott SM, Topham MK. Diacylglycerol kinase zeta regulates phosphatidylinositol 4-phosphate 5-kinase Iα by a novel mechanism. *Cell Signal* 2004;**16**:891−7.
41. Olenchock BA, Guo R, Silverman MA, Wu JN, Carpenter JH, Koretzky GA, et al. Impaired degranulation but enhanced cytokine production after Fc epsilonRI stimulation of diacylglycerol kinase zeta-deficient mast cells. *J Exp Med* 2006;**203**:1471−80.
42. Schubert N, Kirchhoff D, Zeidan J, Duchesne J, Boulais P, Ishii Y. Phosphorylated extracellular signal-regulated kinase (pERK) activation in T effector cells as a target engagement biomarker for the DGKζ inhibitor BAY2965501 in clinical trials. *Cancer Res* 2023;**83**(7_Supplement):2116.
43. Chen X, Wong YK, Wang J, Zhang J, Lee YM, Shen HM, et al. Target identification with quantitative activity based protein profiling (ABPP). *Proteomics* 2017;**17**:1600212.
44. Zhu Y, Ouyang Z, Du H, Wang M, Wang J, Sun H, et al. New opportunities and challenges of natural products research: when target identification meets single-cell multiomics. *Acta Pharm Sin B* 2022;**12**:4011−39.
45. Zhong XP, Hainey EA, Olenchock BA, Jordan MS, Maltzman JS, Nichols KE, et al. Enhanced T cell responses due to diacylglycerol kinase zeta deficiency. *Nat Immunol* 2003;**4**:882−90.
46. Gu J, Wang C, Cao C, Huang J, Holzhauer S, Desilva H, et al. DGKζ exerts greater control than DGKα over $CD8^+$ T cell activity and tumor inhibition. *OncoImmunology* 2021;**10**:1941566.
47. Olenchock BA, Guo R, Carpenter JH, Jordan M, Topham MK, Koretzky GA, et al. Disruption of diacylglycerol metabolism impairs the induction of T cell anergy. *Nat Immunol* 2006;**7**:1174−81.
48. Yang J, Wang HX, Xie J, Li L, Wang J, Wan ECK, et al. DGK α and ζ activities control TH1 and TH17 cell differentiation. *Front Immunol* 2020;**10**:3048.
49. Liu CH, Machado FS, Guo R, Nichols KE, Burks AW, Aliberti JC, et al. Diacylglycerol kinase zeta regulates microbial recognition and host resistance to Toxoplasma gondii. *J Exp Med* 2007;**204**:781−92.
50. Iwazaki K, Tanaka T, Hozumi Y, Okada M, Tsuchiya R, Iseki K, et al. DGKζ downregulation enhances osteoclast differentiation and bone resorption activity under inflammatory conditions. *J Cell Physiol* 2017;**232**:617−24.
51. Zamani A, Decker C, Cremasco V, Hughes L, Novack DV, Faccio R. Diacylglycerol kinase ζ (DGKζ) is a critical regulator of bone homeostasis *via* modulation of c-Fos levels in osteoclasts. *J Bone Miner Res* 2015;**30**:1852−63.
52. Mahajan S, Mellins ED, Faccio R. Diacylglycerol kinase ζ regulates macrophage responses in juvenile arthritis and cytokine storm syndrome mouse models. *J Immunol* 2020;**204**:137−46.
53. Viatour P, Merville MP, Bours V, Chariot A. Phosphorylation of NF-κB and IkappaB proteins: implications in cancer and inflammation. *Trends Biochem Sci* 2005;**30**:43−52.
54. Kim SH, Park SY, Park YL, Myung DS, Rew JS, Joo YE. Chlorogenic acid suppresses lipopolysaccharide-induced nitric oxide and interleukin-1β expression by inhibiting JAK2/STAT3 activation in RAW264.7 cells. *Mol Med Rep* 2017;**16**:9224−32.
55. Hsieh WY, Zhou QD, York AG, Williams KJ, Scumpia PO, Kronenberger EB, et al. Toll-like receptors induce signal-specific reprogramming of the macrophage lipidome. *Cell Metab* 2020;**32**:128−43.e5.
56. Zhao Y, Sun H, Li X, Liu Q, Liu Y, Hou Y, et al. DGKZ promotes TGFβ signaling pathway and metastasis in triple-negative breast cancer by suppressing lipid raft-dependent endocytosis of TGFβR2. *Cell Death Dis* 2022;**13**:105.
57. Baldanzi G, Ragnoli B, Malerba M. Potential role of diacylglycerol kinases in immune-mediated diseases. *Clin Sci (Lond)* 2020;**134**:1637−58.
58. Sakane F, Hoshino F, Murakami C. New era of diacylglycerol kinase, phosphatidic acid and phosphatidic acid-binding protein. *Int J Mol Sci* 2020;**21**:6794.
59. Kadamur G, Ross EM. Mammalian phospholipase C. *Annu Rev Physiol* 2013;**75**:127−54.
60. Zhang F, Zhao G, Dong Z. Phosphatidylcholine-specific phospholipase C and D in stimulation of RAW264.7 mouse macrophage-like cells by lipopolysaccharide. *Int Immunopharmacol* 2001;**1**:1375−84.
61. Sharma P, Yadav SK, Shah SD, Javed E, Lim JM, Pan S, et al. Diacylglycerol kinase inhibition reduces airway contraction by negative feedback regulation of Gq-signaling. *Am J Respir Cell Mol Biol* 2021;**65**:658−71.